

**POLITECNICO DI TORINO**

**Master's Degree in Nanotechnologies for ICTs**



**Master's Degree Thesis**

**MODELING OF DOUBLE-PASS AMPLIFICATION  
IN QUANTUM DOT SEMICONDUCTOR  
AMPLIFIERS**

**Supervisors**

**Prof. Paolo BARDELLA**

**Candidate**

**Pierluigi ANTONACI**

**December 2020**



# Summary

Quantum Dots, due to their three-dimensional quantum confinement, have an electronic structure comparable to the one of atoms. This allows to have a small set of interband transitions with well-defined characteristic energies. Moreover, due to their small DOS, inversion is reached at low injections rate, thus making them a viable candidate for active medium in optoelectronics.

The implementation of multiple – electrically isolated contact regions in a single SOA has allowed for a fine tuning of the output power and spectrum, by means of the gain, in each section.

In this work these two concepts are combined at first to show the obtainable spectral asymmetry (and its tunability) that can be achieved with a single tapered device; at last the same device is simulated in a double-pass configuration. For this a self-consistent time-domain travelling-wave model is developed.



# Table of Contents

<b>List of Tables</b>	VI
<b>List of Figures</b>	VII
<b>1 Thesis outline</b>	1
<b>2 QD based optoelectronic devices</b>	4
2.1 Quantum Dot fabrication . . . . .	4
2.2 Wave propagation . . . . .	6
2.3 Rate equations . . . . .	8
2.4 QD Optical Response . . . . .	12
2.4.1 Spontaneous emission noise . . . . .	13
<b>3 TDTW description</b>	15
3.1 Time stepped solution . . . . .	16
3.2 Numerical modelling of the spontaneous emission noise . . . . .	17
3.3 Summary . . . . .	18
<b>4 Model implementation</b>	19
4.1 Reference frequency and time step . . . . .	20
4.2 Physical parameters . . . . .	21
<b>5 Tunable spectral asymmetry</b>	22
<b>6 Double-Pass amplification</b>	29
<b>7 Conclusions</b>	35
<b>A Code implementations</b>	36
A.1 Modelling chirped QD . . . . .	36
A.2 Modeling tapered structures . . . . .	42
A.3 Modeling multiple electrodes . . . . .	43

A.4	Modeling the external feedback . . . . .	44
A.5	Carriers variation . . . . .	45
A.6	Reference energy . . . . .	51
	<b>Bibliography</b>	54

# List of Tables

4.1	Physical parameters . . . . .	21
5.1	Occupation probability of the 3 considered QD groups in the rear section for the 0.1/1 Å setup. . . . .	23
5.2	Occupation probability of the 3 considered QD groups in the front section for the 0.1/1 Å setup. . . . .	23
5.3	Occupation probability of the 3 considered QD groups in the rear section for the 0.1/3.5 Å setup. . . . .	25
5.4	Occupation probability of the 3 considered QD groups in the front section for the 0.1/3.5 Å setup. . . . .	26
A.1	Reference energy without considering multiplicity (center) and considering it (right) for the simulated device . . . . .	52
A.2	Reference energy without considering multiplicity (center) and considering it (right) with the simulated chirped structure, but with greater asymmetry between the number of layers in each group . . . . .	52
A.3	Reference energy without considering multiplicity (center) and considering it (right) with great asymmetry between the number of layers in each group and with greater asymmetry in the energy levels . . . . .	53

# List of Figures

1.1	Simulated Device, courtesy of [5] . . . . .	2
1.2	Amplifier configurations, from [6] Fig. 2 . . . . .	2
2.1	Optical fiber attenuation [11] . . . . .	5
4.1	Schematic representation of the epitaxial structure, courtesy of [5] . . . . .	19
5.1	Occupation probability in the rear (a) and front (b) section for the 0.1/1 A setup . . . . .	23
5.2	Gain spectra in the rear and front section for the 0.1/1 A setup . . . . .	24
5.3	Simulation results for the 0.1/1 A setup, courtesy of [5] . . . . .	24
5.4	Output spectra in the rear and front section for the 0.1/1 A setup . . . . .	25
5.5	Occupation probability in the rear (a) and front (b) section for the 0.1/3.5 A setup . . . . .	26
5.6	Gain spectra in the rear and front section for the 0.1/3.5 A setup . . . . .	27
5.7	Simulation results for the 0.1/3.5 A setup, courtesy of [5] . . . . .	27
5.8	Output spectra in the rear and front section for the 0.1/3.5 A setup . . . . .	28
6.1	Output power for the single pass configuration . . . . .	29
6.2	Gain for the single pass configuration . . . . .	30
6.3	Experimental gain for the single pass configuration, courtesy of [6] . . . . .	30
6.4	Output power for the double pass configuration . . . . .	31
6.5	Gain for the double pass configuration . . . . .	31
6.6	Experimental gain for the double pass configuration, courtesy of [6] . . . . .	32
6.7	Output power for both configurations at fixed rear current of 0.1A . . . . .	32
6.8	Gain for both configurations at fixed rear current of 0.1A . . . . .	33
6.9	Output power spectra of both configurations at increasing front current . . . . .	34
A.1	Distribution of the existence probability obtained with A.4 . . . . .	40
A.2	Distribution of the existence probability obtained with A.5 . . . . .	41
A.3	Width as a function of the longitudinal position $z$ . . . . .	43



# Chapter 1

## Thesis outline

With the continuous progress of epitaxial growth techniques of the last decades, there has been a growing interest in low-dimensional systems (2D, 1D and 0D), where the de Broglie wavelength of the electron:

$$\lambda_{dB} = \frac{\hbar}{(2mE)^{1/2}} \quad (1.1)$$

is comparable with the characteristic length of the quantum structure in one or more directions. These low dimensional systems, in the form of quantum wells (2D), quantum wires (1D) and quantum dots (0D) cannot be treated with the classical Boltzmann equation. One of the most notable feature of a low dimensional system comes in its density of states, which greatly differs from their classical 3D counterpart. For a 2D system we have a constant DOS for every subband, with a value of:

$$g_{2D} = \frac{m^*}{\pi\hbar^2} \quad (1.2)$$

The 1D density of states, instead can be written as:

$$D^{1D}(E) = \frac{1}{2\pi} \left( \frac{2m^*}{\hbar^2} \right)^{1/2} (E - E_n)^{-1/2} \quad (1.3)$$

Where  $E_n$  represents the confined states of the system ( $n = 1, 2, 3, \dots$ ). On the other hand Quantum Dots have a peculiar density of states due to their 3D confinement. At a first approximation it can be considered as an ensemble of Dirac delta-like density of states. For this reason quantum dots are usually referred to as artificial atoms. Quantum Dots based optoelectronic devices have shown great capabilities in several applications ([1, 2, 3]) due to their peculiar density of states that allows for fast gain recovery times. In this thesis an existing TDTW model ([4]) is expanded to allow for the simulation of chirped QD active materials, using as reference the experimental results obtained for

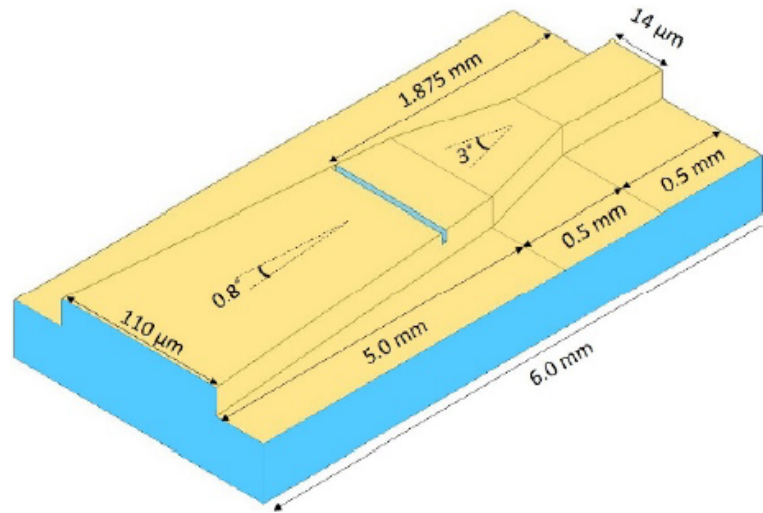


**Figure 1.1:** Simulated Device, courtesy of [5]

the device depicted in Fig. 1.1 and experimentally measured by [5, 6]. The shown device is a quantum-dot based amplifier with a tapered shape: this allows for a good beam quality while granting for an increased active region with respect to a configuration with constant width. The active region of the device is made up of three groups of InAs QDs, for a total of ten layers. Due to the chirped structure each QD group has a different ground state emission wavelength. The main objective of this work is to properly model the Double-Pass amplification presented in [6], where the device has been measured in the two conditions shown in Fig. 1.2.

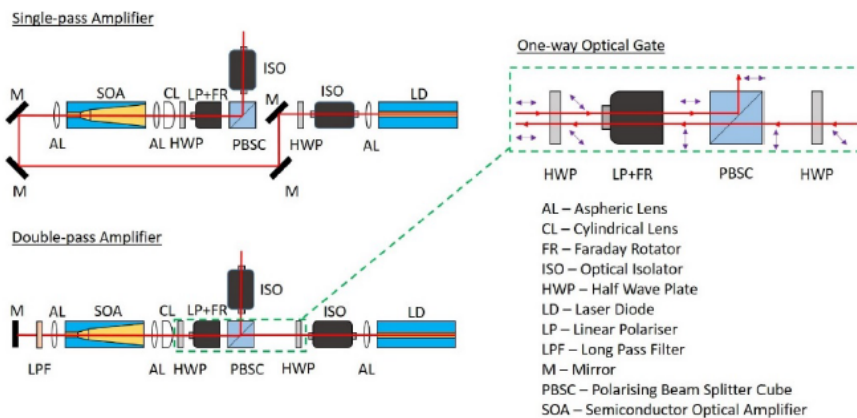


**Figure 1.2:** Amplifier configurations, from [6] Fig. 2

In chapter 2 the fundamental theory needed to study QD-based optoelectronic

---

devices is presented, then integrated with the implemented Time Domain Travelling Wave Model in chapter 3. All the model and physical parameters are then presented in chapter 4 along the with the numerical implementations of specific features of the simulated device. Lastly in chapters 5 and 6 simulation results are presented, along with their experimental counterparts.

## Chapter 2

# QD based optoelectronic devices

The model used to perform simulations on the aforementioned device is the Time Domain Travelling Wave model. It relies on the direct solution of the travelling wave equations using a finite difference method. The first aspect that has to be defined is the propagation of the field in the device, this can be described by the following second-order differential equation [4]:

$$\frac{\partial^2 \vec{V}}{\partial z^2} - \frac{1}{c^2} \frac{\partial^2}{\partial t^2} (\eta^2 \vec{V}) = \mu_0 \frac{\partial^2 \vec{P}}{\partial t^2} + \mu_0 \frac{\partial \vec{J}}{\partial t} \quad (2.1)$$

where  $V(z, T)$  refers to the amplitude of the TE guided mode. In this model both transverse magnetic modes and high order TE modes are not taken into account. This approximation derives directly from practical applications, since the grand majority of optoelectronic devices are engineered to only support the first guided mode at operating frequency, while all higher order modes are below cutoff ([7] [8]). The two key factors that define the behaviour of the medium are:

1.  $\vec{P}$ : the additional polarization induced by the active material
2.  $\vec{J}$ : a stochastic current density that models the spontaneous emission noise from the active medium

In the following sections the main equations used for modelling quantum dot based optoelectronic devices are discussed.

### 2.1 Quantum Dot fabrication

The continuous progress in fabrication techniques has allowed the possibility of growing quantum dots ensembles of III-V semiconductor compounds. These materials (GaAs or

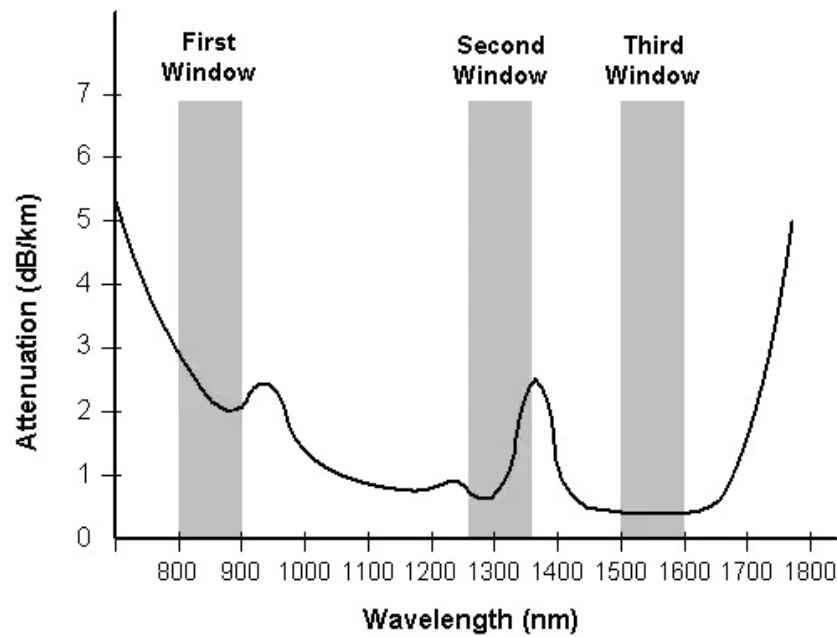


**Figure 2.1:** Optical fiber attenuation [11]

InAs, to list two) are key for optoelectronics, due to their emission wavelengths that span from  $1\mu\text{m}$  to  $1.8\mu\text{m}$ , thus covering most of the window used in telecommunication applications.

The main technique used for the growth of III-V QDs is molecular beam epitaxy (MBE) ([9] [10]), combined with a layer-island growth (Stranski-Krastanov (SK) process). Quantum Dots grown by these means can be tuned in size, shape, dimensions and density by controlling the growth parameters.

The high tunability of this process, and therefore of the grown structure, highly impacts the potential profile of the quantum dots, and, consequentially, the electronic and optical properties of the grown quantum dots.

As every growth process, also the SK method is subject to fluctuations that lead to dispersions in the so grown QD characteristics. The most notable influence of these fluctuations is found in the density of states of the quantum dots: the Dirac delta-like shape is influenced by an inhomogeneous broadening that directly leads to a gain spectra with a defined bandwidth.

Several compounds have been used in optoelectronic devices as active materials due to the fact that their emission wavelengths fall in one windows where attenuation is lower in an optical fiber (Fig. 2.1): for example InAs and  $\text{In}_x\text{Ga}_{1-x}\text{As}$  ([12], [13]) can be implemented for the second window while for the third InAs/InP are available ([14]).

Since when grown by the SK process QDs are subjected to variance, it is possible to define a Gaussian distribution that describes the probability of the  $i$ -th QD to have a

specific GS transition energy:

$$G_i = 1/Z \exp\left(-4 \log 2 \frac{\hbar\omega_{i,GS} - \hbar\omega_{(N+1)/2,GS}}{\Delta E^2}\right) \quad (2.2)$$

where the normalization constant  $Z$  has been defined in order to ensure that  $\sum_i G_i = 1$ .

After reviewing the most common technique used to grow QD, in this section a distribution has been defined to properly model an ensemble of self-assembled quantum dots; in the next section a proper description of wave propagation in a waveguide will be given.

## 2.2 Wave propagation

The fundamental theory of wave propagation in a waveguide has been studied and developed by Marcuvitz and Schwinger ([15, 16]), starting from the Maxwell equations the Electric and Magnetic field in the frequency domain ( $\omega$ ):

$$\nabla \times \vec{E} = -j\omega\mu_0\vec{H} \quad (2.3a)$$

$$\nabla \times \vec{H} = j\omega\epsilon_0\epsilon(\omega, \vec{r})\vec{E} + j\omega\vec{P}(\omega, \vec{r}) + \vec{J}(\omega, \vec{r}) \quad (2.3b)$$

where we can find the frequency-domain counterparts of the previously highlighted terms that define the optical response of the active medium. Starting from this coupled equations, the travelling wave equations can be defined. In order to do so a linear response of the active material is assumed, thus the polarization term  $\vec{P}$  can be expressed as:

$$\vec{P}(\omega, \vec{r}) = \epsilon_0 \underline{\underline{\chi}}(\omega, \vec{r}) \vec{E}(\omega, \vec{r}) \quad (2.4)$$

where  $\underline{\underline{\chi}}(\omega, \vec{r})$  is the material electronic susceptibility. From a theoretical point of view this susceptibility is a non-diagonal matrix, that takes in account the anisotropy of the optical response of the material, but, as will be shown later, optical transitions for quantum dots are mainly located along the in plane axis. By expressing all the vectorial components in terms of their longitudinal and transverse components,  $\vec{A} = \vec{A}_t + A_z \hat{z}$ , the Marcuvitz-Schwinger equations are obtained:

$$\frac{\partial \vec{E}_t}{\partial z} = j\omega\mu_0 \left[ \mathbb{1} + \frac{c^2}{\omega^2} \nabla_t \frac{1}{\epsilon} \nabla_t \right] (\vec{H}_t \times \hat{z}) - \nabla_t \frac{P_z}{\epsilon_0 \epsilon} - \nabla_t \frac{J_z}{j\omega\epsilon_0 \epsilon} \quad (2.5a)$$

$$\frac{\partial \vec{H}_t}{\partial z} = j\omega\epsilon_0 \left[ \epsilon \mathbb{1} + \frac{c^2}{\omega^2} \nabla_t \nabla_t \right] (\hat{z} \times \vec{E}_t) + j\omega (\hat{z} \times \vec{P}_t) + \hat{z} \times \vec{J}_t \quad (2.5b)$$

The solutions for this equations are both guided modes and radiation modes, but as stated before, only the first guided mode is considered. By introducing the slowly varying envelope approximation (SVEA), also referred to as narrow-band approximation,

due to the fact that it assumes that the envelope of a travelling wave slowly varies when compared to the wavelength of its central frequency ( $\omega_0$ ), the amplitude in the time-domain can be expressed as:

$$V(z, t) = \sqrt{2 \frac{\omega_0 \mu_0}{\beta_0}} \{V^+(z, t)e^{-j\beta_0 z} + V^-(z, t)e^{-j\beta_0 z}\} e^{j\omega_0 t} \quad (2.6)$$

Where  $V^+(z, t)$  and  $V^-(z, t)$  are the forward and backward propagating terms.  $\omega_0$  is the reference frequency and  $\beta_0$  is the corresponding propagation constant  $\beta_0 = \beta(\omega_0) = \frac{\omega_0}{c} \eta_0$  with  $\eta_0 = \eta(\omega_0)$ . In frequency domain expression 2.6 becomes:

$$V(z, \omega_0 + \Omega) = \sqrt{2 \frac{\omega_0 \mu_0}{\beta_0}} \{V^+(z, \Omega)e^{-j\beta_0 z} + V^-(z, \Omega)e^{-j\beta_0 z}\} \quad (2.7)$$

with the variable change  $\Omega = \omega - \omega_0$ . Assuming  $\left| \beta_0 \frac{\partial V^\pm}{\partial z} \right| \gg \left| \frac{\partial^2 V^\pm}{\partial z^2} \right|$  and keeping only first order terms in  $\Omega$ :

$$\begin{aligned} \pm \frac{\partial V^\pm}{\partial z}(z, \Omega) &= -j \frac{\Omega}{v_{g0}} V^\pm(z, \Omega) - j \frac{\omega_0}{2c\eta_0} \Gamma_{xy} \tilde{\chi}(\omega_0 + \Omega, z) V^\pm(z, \Omega) + \\ &+ \frac{1}{2} \sqrt{\frac{\mu_0 \omega_0}{2\beta_0}} J(\omega_0 + \Omega, z) \end{aligned} \quad (2.8)$$

where the group velocity has been defined as:

$$\frac{1}{v_{g0}} = \frac{\eta_0}{c} \left( 1 + \frac{\omega_0}{\eta_0} \frac{\partial \eta}{\partial \omega} \Big|_{\omega_0} \right) \quad (2.9)$$

and  $\Gamma_{xyi}$  is the field confinement factor, which represents the overlap between the guided mode and the active medium, and is defined in Eq. 2.10:

$$\Gamma_{xyi} \tilde{\chi}(z, \omega) = \iint \chi(x, y, z, \omega) |V|^2(x, y) dx dy \quad (2.10)$$

Antitransforming equations (2.8), two independent first order time-domain equations for the forward and backward propagating amplitudes are obtained:

$$\pm \frac{\partial V^\pm}{\partial z} + \frac{1}{v_{g0}} \frac{\partial V^\pm}{\partial t} = -\frac{\alpha_i}{2} V^\pm - j \frac{\omega_0}{2c\eta_0 \epsilon_0} \Gamma_{xy} P^\pm(z, t) + F^\pm(z, t) \quad (2.11)$$

where slowly varying forward and backward traveling polarization terms  $P^\pm(z, t)$  have been defined as:

$$P^\pm(z, t) = \epsilon_0 \bar{\chi}(t, z) \otimes V^\pm(t, z) = \epsilon_0 \int_{-\infty}^t \bar{\chi}(t - \tau, z) V^\pm(z, \tau) d\tau \quad (2.12a)$$

$$\bar{\chi}(t, z) = \frac{1}{2\pi} \int_{-\infty}^{+\infty} \tilde{\chi}(\omega_0 + \Omega, z) e^{j\Omega t} d\Omega = \tilde{\chi}(t, z) e^{-j\omega_0 t} \quad (2.12b)$$

Similarly, the spontaneous emission noise sources  $F^\pm(z, t)$  for forward and backward travelling components can be defined:

$$\begin{aligned} F^\pm(z, t) &= \frac{1}{2} \sqrt{\frac{\mu_0 \omega_0}{2\beta_0}} \frac{1}{2\pi} \int_{-\infty}^{+\infty} J(\omega_0 + \Omega, z) e^{j\Omega t} d\Omega = \\ &= \frac{1}{2} \sqrt{\frac{\mu_0 \omega_0}{2\beta_0}} J(t, z) e^{-j\omega_0 t} \end{aligned} \quad (2.13)$$

A key term that will be used to properly model the device treated in this work is the intrinsic waveguide losses  $\alpha_i$ , that takes into account for additional losses in the waveguide. Even though in this derivation this parameter is treated as independent from the propagation direction (forward or backward) in order to simplify the treatment of the analyzed device it will be split into a progressive losses term ( $\alpha^+$ ) and a regressive losses term ( $\alpha^-$ ).

The instantaneous optical power in a given section  $z$  of the waveguide can be written as:

$$S(z, t) = S^+(z, t) - S^-(z, t) = |V^+|^2(z, t) - |V^-|^2(z, t) \quad (2.14)$$

and the corresponding optical power per unit bandwidth as:

$$\begin{aligned} S(z, \omega) &= S^+(z, \omega) - S^-(z, \omega) \\ &= |V^+|^2(z, \omega - \omega_0) - |V^-|^2(z, \omega - \omega_0) \end{aligned} \quad (2.15)$$

A differential equation for  $S^\pm(z, \omega)$  can be obtained by multiplying (2.8) by  $V^{\pm*}$  and adding the complex conjugate of the same resulting equation, obtaining:

$$\frac{\partial S^\pm(z, \omega)}{\partial z} = (\Gamma_{xy} g(z, \omega) - \alpha_i) S^\pm(z, \omega) + |F^\pm(z, \omega - \omega_0)|^2 \quad (2.16)$$

where  $g(z, \omega)$  represents the gain induced by the active medium:

$$g(z, \omega) = \frac{\omega_0}{c\eta_0} \text{Im} \{ \tilde{\chi}(z, \omega) \} \quad (2.17)$$

In this section the fundamental theory of wave propagation in a waveguide has been defined, in the next one the rate equations that govern the carrier dynamics in the active medium will be defined in order to obtain a complete description of quantum dot-based optoelectronic devices.

## 2.3 Rate equations

In order to properly model the carriers dynamics scattering rates deriving from the density matrix theory. Two types of scattering rates can be defined:

- In and out scattering rates
- Recombination rates

The first one, since it must take into account the Pauli exclusion principle, can be written as:

$$R_{\lambda,k' \rightarrow k} (f_{\lambda,k}^i, f_{\lambda,k'}^i) = \frac{f_{\lambda,k'}^i(z, t) (1 - f_{\lambda,k}^i(z, t))}{\tau_{k' \rightarrow k}} \quad (2.18)$$

where  $\tau_{k' \rightarrow k}$  describes the strength of the scattering process. Since without external perturbation the carriers would tend to a quasi-equilibrium distribution, a relation between  $R_{\lambda,k' \rightarrow k} (f_{\lambda,k}^i, f_{\lambda,k'}^i)$  and its reverse process  $R_{\lambda,k \rightarrow k'} (f_{\lambda,k'}^i, f_{\lambda,k}^i)$  must be imposed. This is done by imposing the following relation between the time constants:

$$\frac{\tau_{k \rightarrow k'}}{\tau_{k' \rightarrow k}} = \exp\left(\frac{\varepsilon_{\lambda,k'}^i - \varepsilon_{\lambda,k}^i}{k_B T}\right) \quad (2.19)$$

In this treatment three recombination rates are considered: spontaneous emission, non-radiative recombination and Auger recombination. The first one can be defined as:

$$R_k^{sp} (f_{e,k}^i, f_{h,k}^i) = \frac{1}{\tau_{sp,k}} f_{e,k}^i f_{h,k}^i \quad (2.20)$$

similarly, the non-radiative process can be written as:

$$R_{\lambda,k}^{nr} = \frac{f_{\lambda,k}^i}{\tau_{nr,k}} \quad (2.21)$$

Auger recombination rates usually require a more in depth analysis, as shown in [17], and in this work they will be defined as shown in (2.22):

$$\begin{aligned} R_{e,k}^{Aug} &= \frac{1}{\tau_{Aug,k}} (f_{e,k}^i)^2 f_{h,k}^i + \frac{1}{2} \frac{1}{\tau_{Aug,k}} (f_{h,k}^i)^2 f_{e,k}^i \\ R_{h,k}^{Aug} &= \frac{1}{\tau_{Aug,k}} (f_{h,k}^i)^2 f_{e,k}^i + \frac{1}{2} \frac{1}{\tau_{Aug,k}} (f_{e,k}^i)^2 f_{h,k}^i \end{aligned} \quad (2.22)$$

Now that all the scattering mechanism have been defined the rate equations for SCH, WL, ES2, ES1 and GS can be written:

$$\begin{aligned} \frac{\partial n_{\lambda,SCH}}{\partial t} &= \eta_i \frac{J}{e} W - \frac{n_{\lambda,SCH}}{\tau_{SCH \rightarrow QW}^\lambda} + \frac{n_{\lambda,QW}}{\tau_{QW \rightarrow SCH}^\lambda} \\ &\quad - \frac{B_{SCH}}{W \cdot h_{SCH}} n_{e,SCH} n_{h,SCH} - \frac{n_{\lambda,SCH}}{\tau_{nr,SCH}^\lambda} \end{aligned} \quad (2.23)$$

$$\begin{aligned}
 \frac{\partial n_{\lambda,QW}}{\partial t} &= \frac{n_{\lambda,SCH}}{\tau_{SCH \rightarrow QW}^\lambda} - \frac{n_{\lambda,QW}}{\tau_{QW \rightarrow SCH}^\lambda} - \frac{B_{QW}}{W \cdot h_w} n_{e,QW} n_{h,QW} - \frac{n_{\lambda,QW}}{\tau_{nr,QW}^\lambda} \\
 &+ \sum_{i=1}^N \frac{G_i}{\tau_{QW \rightarrow ES_2}^\lambda} n_{QW} (1 - \tilde{f}_{\lambda,ES_2}^i) + \sum_{i=1}^N \frac{n_{\lambda,ES_2}^i}{\tau_{ES_2 \rightarrow QW}^\lambda}
 \end{aligned} \tag{2.24}$$

$$\begin{aligned}
 \frac{\partial n_{\lambda,ES_2}^i}{\partial t} &= \frac{G_i}{\tau_{QW \rightarrow ES_2}^\lambda} n_{QW} (1 - \tilde{f}_{\lambda,ES_2}^i) - \frac{n_{\lambda,ES_2}^i}{\tau_{ES_2 \rightarrow QW}^\lambda} \\
 &- \frac{n_{\lambda,ES_2}^i}{\tau_{ES_2 \rightarrow ES_1}^\lambda} (1 - \tilde{f}_{\lambda,ES_1}^i) + \frac{n_{\lambda,ES_1}^i}{\tau_{ES_1 \rightarrow ES_2}^\lambda} (1 - \tilde{f}_{\lambda,ES_2}^i) \\
 &- \frac{n_{e,ES_2}^i \tilde{f}_{h,ES_2}^i}{\tau_{sp,ES_2}} - \frac{\tilde{f}_{e,ES_2}^i \tilde{f}_{h,ES_2}^i}{\tau_{Aug,ES_2}} \left( n_{\lambda,ES_2}^i + \frac{1}{2} n_{\lambda' \neq \lambda,ES_2}^i \right) \\
 &- \frac{n_{\lambda,ES_2}^i}{\tau_{nr,ES_2}^\lambda} - R_{st,ES_2}^i
 \end{aligned} \tag{2.25}$$

$$\begin{aligned}
 \frac{\partial n_{\lambda,ES_1}^i}{\partial t} &= \frac{n_{\lambda,ES_2}^i}{\tau_{ES_2 \rightarrow ES_1}^\lambda} (1 - \tilde{f}_{\lambda,ES_1}^i) - \frac{n_{\lambda,ES_1}^i}{\tau_{ES_1 \rightarrow ES_2}^\lambda} (1 - \tilde{f}_{\lambda,ES_2}^i) \\
 &- \frac{n_{\lambda,ES_1}^i}{\tau_{ES_1 \rightarrow GS}^\lambda} (1 - \tilde{f}_{\lambda,GS}^i) + \frac{n_{\lambda,GS}^i}{\tau_{GS \rightarrow ES_1}^\lambda} (1 - \tilde{f}_{\lambda,ES_1}^i) \\
 &- \frac{n_{e,ES_1}^i \tilde{f}_{h,ES_1}^i}{\tau_{sp,ES_1}} - \frac{\tilde{f}_{e,ES_1}^i \tilde{f}_{h,ES_1}^i}{\tau_{Aug,ES_1}} \left( n_{\lambda,ES_1}^i + \frac{1}{2} n_{\lambda' \neq \lambda,ES_1}^i \right) \\
 &- \frac{n_{\lambda,ES_1}^i}{\tau_{nr,ES_1}^\lambda} - R_{st,ES_1}^i
 \end{aligned} \tag{2.26}$$

$$\begin{aligned}
 \frac{\partial n_{\lambda,GS}^i}{\partial t} &= \frac{n_{\lambda,ES_1}^i}{\tau_{ES_1 \rightarrow GS}^\lambda} (1 - \tilde{f}_{\lambda,GS}^i) - \frac{n_{\lambda,GS}^i}{\tau_{GS \rightarrow ES_1}^\lambda} (1 - \tilde{f}_{\lambda,ES_1}^i) \\
 &- \frac{n_{e,GS}^i \tilde{f}_{h,GS}^i}{\tau_{sp,GS}} - \frac{\tilde{f}_{e,GS}^i \tilde{f}_{h,GS}^i}{\tau_{Aug,GS}} \left( n_{\lambda,GS}^i + \frac{1}{2} n_{\lambda' \neq \lambda,GS}^i \right) \\
 &- \frac{n_{\lambda,GS}^i}{\tau_{nr,GS}^\lambda} - R_{st,GS}^i
 \end{aligned} \tag{2.27}$$

the only term that is not defined is the stimulated emission rate that will be defined in the following section, since it relies on an approximation that has not been introduced yet. In (2.23) and (2.24), coefficients  $B_{SCH}$  and  $B_{QW}$  represent the strength of the spontaneous emission from the SCH and QW states. The applied current density is represented by  $J$  in 2.23 whereas  $\eta_i$  is the internal quantum efficiency. A common approximation ([18, 19, 20, 21]) is the excitonic one, where charge neutrality is assumed in every QD state, as well as in the SCH and in the quantum well. This allows to further simplify the rate equations, that in the excitonic approach are the following:

$$\begin{aligned} \frac{\partial n_{SCH}}{\partial t} = & \eta_i \frac{J}{e} W - \frac{n_{SCH}}{\tau_{SCH \rightarrow QW}} + \frac{n_{QW}}{\tau_{QW \rightarrow SCH}} \\ & - \frac{B_{SCH}}{W \cdot h_{SCH}} n_{SCH}^2 - \frac{n_{SCH}}{\tau_{nr, SCH}} \end{aligned} \quad (2.28)$$

$$\begin{aligned} \frac{\partial n_{QW}}{\partial t} = & \frac{n_{SCH}}{\tau_{SCH \rightarrow QW}} - \frac{n_{QW}}{\tau_{QW \rightarrow SCH}} - \frac{B_{QW}}{W \cdot h_w} n_{QW}^2 - \frac{n_{QW}}{\tau_{nr, QW}} \\ & + \sum_{i=1}^N \frac{G_i}{\tau_{QW \rightarrow ES_2}} n_{QW} (1 - \tilde{f}_{ES_2}^i) + \sum_{i=1}^N \frac{n_{ES_2}^i}{\tau_{ES_2 \rightarrow QW}} \end{aligned} \quad (2.29)$$

$$\begin{aligned} \frac{\partial n_{ES_2}^i}{\partial t} = & \frac{G_i}{\tau_{QW \rightarrow ES_2}} n_{QW} (1 - \tilde{f}_{ES_2}^i) - \frac{n_{ES_2}^i}{\tau_{ES_2 \rightarrow QW}^i} \\ & - \frac{n_{ES_2}^i}{\tau_{ES_2 \rightarrow ES_1}} (1 - \tilde{f}_{ES_1}^i) + \frac{n_{ES_1}^i}{\tau_{ES_1 \rightarrow ES_2}} (1 - \tilde{f}_{ES_2}^i) \\ & - \frac{n_{ES_2}^i}{\tau_{sp, ES_2}} - \frac{n_{ES_2}^i \tilde{f}_{ES_2}^i}{\tau_{Aug, ES_2}} - \frac{n_{ES_2}^i}{\tau_{nr, ES_2}} - R_{st, ES_2}^i \end{aligned} \quad (2.30)$$

$$\begin{aligned} \frac{\partial n_{ES_1}^i}{\partial t} = & \frac{n_{ES_2}^i}{\tau_{ES_2 \rightarrow ES_1}} (1 - \tilde{f}_{ES_1}^i) - \frac{n_{ES_1}^i}{\tau_{ES_1 \rightarrow ES_2}} (1 - \tilde{f}_{ES_2}^i) \\ & - \frac{n_{ES_1}^i}{\tau_{ES_1 \rightarrow GS}} (1 - \tilde{f}_{GS}^i) + \frac{n_{GS}^i}{\tau_{GS \rightarrow ES_1}} (1 - \tilde{f}_{ES_1}^i) \\ & - \frac{n_{ES_1}^i}{\tau_{sp, ES_1}} - \frac{n_{ES_1}^i \tilde{f}_{ES_1}^i}{\tau_{Aug, ES_1}} - \frac{n_{\lambda, ES_1}^i}{\tau_{nr, ES_1}} - R_{st, ES_1}^i \end{aligned} \quad (2.31)$$

$$\begin{aligned} \frac{\partial n_{GS}^i}{\partial t} = & \frac{n_{ES_1}^i}{\tau_{ES_1 \rightarrow GS}} (1 - \tilde{f}_{GS}^i) - \frac{n_{GS}^i}{\tau_{GS \rightarrow ES_1}} (1 - \tilde{f}_{ES_1}^i) \\ & - \frac{n_{GS}^i}{\tau_{sp,GS}} - \frac{n_{GS}^i \tilde{f}_{h,GS}^i}{\tau_{Aug,GS}} - \frac{n_{GS}^i}{\tau_{nr,GS}} - R_{st,GS}^i \end{aligned} \quad (2.32)$$

In this section the rate equations that have been implemented in the model have been defined, in the next one a proper description of the stimulated emission rate will be given and from that the optical response of the QD-based active material will be determined.

## 2.4 QD Optical Response

From a rigorous description of the QD polarization one could define the polarization as:

$$\begin{aligned} \Gamma_{xy} P^\pm(z, t) = & \Gamma_{xy} \sum_{i=1}^N \sum_k \frac{D_k G_i N_d j |d_{y,k}^i|^2}{h_w \hbar \Gamma} \\ & \mathcal{L}_k^i(t) \otimes [(\tilde{f}_{e,k}^i + \tilde{f}_{h,k}^i - 1) V^\pm(z, t)] \end{aligned} \quad (2.33)$$

where

$$\begin{aligned} \mathcal{L}_k^i(t) \otimes [(\tilde{f}_{e,k}^i + \tilde{f}_{h,k}^i - 1) V^\pm(z, t)] = \\ = \Gamma \int_{-\infty}^t e^{j(\omega_k^i - \omega_0)(t-\tau)} e^{-\Gamma(t-\tau)} (\tilde{f}_{e,k}^i(z, \tau) + \tilde{f}_{h,k}^i(z, \tau) - 1) V^\pm(z, \tau) d\tau \end{aligned} \quad (2.34)$$

but by introducing the adiabatic approximation (which states that a quantum mechanical system that is subjected to perturbations faster than its response time does not respond immediately) it is possible to simplify the convolution integral, and the following expression is obtained for the susceptibility:

$$\bar{\chi}(t, z) = \sum_{i=1}^N \sum_k \frac{D_k G_i N_d j |d_{y,k}^i|^2}{h_w \epsilon_0 \hbar \Gamma} \cdot (\tilde{f}_{e,k}^i(z, t) + \tilde{f}_{h,k}^i(z, t) - 1) \mathcal{L}_k^i(t) \quad (2.35)$$

Equivalently it can be written in the frequency domain as:

$$\bar{\chi}(z, t, \Omega) = \sum_{i=1}^N \sum_k \frac{D_k G_i N_d j |d_{y,k}^i|^2}{h_w \epsilon_0 \hbar \Gamma} \cdot (\tilde{f}_{e,k}^i(z, t) + \tilde{f}_{h,k}^i(z, t) - 1) \mathcal{L}_k^i(\Omega) \quad (2.36)$$

this allows to define the QD gain and the refractive index variation as:

$$\begin{aligned} g(z, t, \Omega) = & \frac{\omega_0}{c \eta_0} \text{Im} \{ \bar{\chi}(z, t, \Omega) \} = \\ = & \sum_{i=1}^N \sum_k g_{0,k}^i (\tilde{f}_{e,k}^i(z, t) + \tilde{f}_{h,k}^i(z, t) - 1) \text{Re} \{ \mathcal{L}_k^i(\Omega) \} \end{aligned} \quad (2.37)$$

$$\begin{aligned}
 \Delta\eta(z, t, \Omega) &= \frac{1}{2\eta_0} \text{Re} \{ \bar{\chi}(z, t, \Omega) \} = \\
 &= \sum_{i=1}^N \sum_k \frac{c}{\omega_0} g_{0,k}^i \cdot (\tilde{f}_{e,k}^i(z, t) + \tilde{f}_{h,k}^i(z, t) - 1) \text{Im} \{ \mathcal{L}_k^i(\Omega) \}
 \end{aligned} \tag{2.38}$$

where  $g_{0,k}^i$  is defined as:

$$g_{0,k}^i = \frac{\omega_0 D_k G_i N_d |d_{y,k}^i|^2}{c\eta_0 \hbar \omega \epsilon_0 \hbar \Gamma} \tag{2.39}$$

What equations 2.36, 2.37 and 2.38 state is that, in the adiabatic approximation, the optical response of the QD-based active material can be modeled by filtering the electromagnetic field through various Lorentzian filters associated to every interband transition of every QD group. These filters have different weights accordingly to the occupation probabilities of each state. This broadening mechanism is referred to as homogeneous broadening. Thanks to these equations it is now possible to express the stimulated emission rate as:

$$\begin{aligned}
 R_{st,k}^i &= \frac{\Gamma_{xy}}{\hbar\omega_0} g_{0,k}^i (\tilde{f}_{e,k}^i(z, t) + \tilde{f}_{h,k}^i(z, t) - 1) \cdot \\
 &\text{Re} \left\{ V^+(z, t) [\mathcal{L}_k^i(t) \otimes V^+(z, t)]^* + V^-(z, t) [\mathcal{L}_k^i(t) \otimes V^-(z, t)]^* \right\}
 \end{aligned} \tag{2.40}$$

thus now we can complete 2.16 by having defined 2.37. By combining 2.40 and 2.14  $R_{st,k}^i$  can be finally written as:

$$\begin{aligned}
 R_{st,k}^i &= \frac{\Gamma_{xy}}{\hbar\omega_0} g_{0,k}^i (\tilde{f}_{e,k}^i(z) + \tilde{f}_{h,k}^i(z) - 1) \cdot \\
 &\int_{-\infty}^{+\infty} \text{Re} \{ \mathcal{L}_k^i(\omega - \omega_0) \} [S^+(z, \omega) + S^-(z, \omega)] d\omega
 \end{aligned} \tag{2.41}$$

where  $S^\pm(z, \omega)$  represents the forward and backward propagating power in the frequency domain defined in 2.15.

### 2.4.1 Spontaneous emission noise

The quantum description of spontaneous emission noise in semiconductors has been developed extensively in several works ([22] and [23]), but for this work it will be obtained by making use of the Einstein theory ([24]). Thanks to the aforementioned theory it is possible to obtain an expression for the spontaneous emitted power per unit length, per unit bandwidth, that is generated from the active material starting from the

gain spectrum of the quantum dot ensemble defined in (2.37):

$$\begin{aligned}
 |F^\pm(z, \Omega)|^2 &= \frac{\beta_{sp}}{2} N_d W N_{lay} \sum_{i=1}^N \sum_k G_i D_k \frac{\Gamma \hbar \omega_k^i}{\pi} R_{sp,k}^i(z, t) \text{Re} \{ \mathcal{L}_k^i(\Omega) \} = \\
 &= \frac{\beta_{sp}}{2} N_d W N_{lay} \sum_{i=1}^N \sum_k G_i D_k \frac{\Gamma \hbar \omega_k^i R_{sp,k}^i(z, t)}{\pi \left( 1 + \left( \frac{\Omega - \omega_k^i + \omega_0}{\Gamma} \right)^2 \right)}
 \end{aligned} \tag{2.42}$$

where  $R_{sp,k}^i$  is the spontaneous emission rate from state  $k$  of the  $i^{th}$  QD group. In order to effectively model the coupling between the spontaneous emission radiation and the guided mode the coefficient  $\beta_{sp}$  is introduced. The characteristic spontaneous emission time  $\tau_{sp,k}$  can be related to the QD gain via the following expression:

$$\begin{aligned}
 (\tau_{sp,k})^{-1} &= \frac{\hbar \omega}{N_d D_k G_i N_{lay}} \frac{\eta_0^2 \omega_k^i{}^2 \Gamma}{\pi c^2} g_{0,k}^i = \\
 &= \frac{|d_{y,k}^i|^2 \eta_0 \omega_k^i{}^3}{\pi c^3 \epsilon_0 \hbar}
 \end{aligned} \tag{2.43}$$

Having defined all the main equations used for modelling quantum dot based optoelectronic devices in this chapter, in the next one an overview of the time domain travelling wave model will be given.

## Chapter 3

# TDTW description

The TDTW model consists in the solution of the travelling wave equation at each time step, by means of a finite difference method: at each time step the optical response of the quantum dots is evaluated. For clarity the key steps used in the numerical model are hereby reported. The set of travelling wave equations that has to be solved can be represented by:

$$\pm \frac{\partial V^\pm}{\partial z} + \frac{1}{v_{g0}} \frac{\partial V^\pm}{\partial t} = -\frac{\alpha_i^\pm}{2} V^\pm - j \frac{\omega_0}{2c\eta_0\epsilon_0} \Gamma_{xy} P^\pm(z, t) + F^\pm(z, t) \quad (3.1)$$

in (3.1) the polarization term is evaluated only for the GS, the first excited state (ES1) and the second excited state (ES2). The term  $P^\pm(z, t)$  represents the forward and backward traveling polarization and can be written as:

$$\Gamma_{xy} P^\pm(z, t) = \Gamma_{xy} \sum_{i=1}^N \sum_{k=GS, ES_1, ES_2} \frac{D_k G_i N_d j |d_{y,k}^i|^2}{h_w \hbar \Gamma} (2\tilde{f}_k^i(z, t) - 1) [\mathcal{L}_k^i(t) \otimes V^\pm(z, t)] \quad (3.2)$$

where the lorentzian filter is needed in order to properly represent the broadening of the interband transitions.  $F^\pm(z, t)$  represents the spontaneous emission noise source, and its power spectral density can be expressed as follows:

$$\begin{aligned} |F^\pm(z, \Omega)|^2 &= \frac{\beta_{sp}}{2} N_d W N_{lay} \sum_{i=1}^N \sum_k G_i D_k \frac{\Gamma \hbar \omega_k^i}{\pi} R_{sp,k}^i(z, t) \text{Re} \{ \mathcal{L}_k^i(\Omega) \} = \\ &= \frac{\beta_{sp}}{2} N_d W N_{lay} \sum_{i=1}^N \sum_k G_i D_k \frac{\Gamma f_{sp,k}^i(z, t)}{\pi \tau_{sp,k}} \frac{\hbar \omega_k^i}{1 + \left( \frac{\Omega - \omega_k^i + \omega_0}{\Gamma} \right)^2} \end{aligned} \quad (3.3)$$

All of these equations must then be coupled with the excitonic rate equations 2.28-2.32. These can be generally expressed as:

$$\frac{\partial n_k^i}{\partial t}(z, t) = R_{in,k}^i(z, t) - R_{out,k}^i(z, t) - R_{rec,k}^i(z, t) - R_{st,k}^i(z, t) \quad (3.4)$$

where the intraband processes are collected in the  $R_{in,k}^i$  and  $R_{out,k}^i$  terms, the recombination term  $R_{rec,k}^i$  collects all the recombinations effects (both radiative and non-radiative) and  $R_{st,k}^i$  represents the stimulated emission. The latter can be expressed as 2.40:

$$R_{st,k}^i = \frac{\Gamma_{xy}}{\hbar\omega_0} g_{0,k}^i (2\tilde{f}_k^i(z, t) - 1) \cdot \text{Re} \left\{ V^+(z, t) [\mathcal{L}_k^i(t) \otimes V^+(z, t)]^* + V^-(z, t) [\mathcal{L}_k^i(t) \otimes V^-(z, t)]^* \right\} \quad (3.5)$$

All of the equations presented in this paragraph have to be solved by a finite difference scheme.

### 3.1 Time stepped solution

The travelling wave equation (3.1) can now be solved. starting from 3.2 and 3.1, it is possible to write:

$$\pm \frac{\partial V^\pm}{\partial z} + j \frac{\Omega}{v_{g0}} V^\pm = \left[ -\frac{\alpha_i}{2} + \Gamma_{xy} \sum_{i=1}^N \sum_{k=GS,ES_1,ES_2} \frac{1}{2} g_{0,k}^i (2\tilde{f}_k^i(z, \Omega) - 1) \otimes \mathcal{L}_k^i(\Omega) \right] V^\pm(z, \Omega) + F^\pm(z, \Omega) = \kappa(z, \Omega) V^\pm(z, \Omega) + F^\pm(z, \Omega)$$

the general solution can be found by first taking the homogeneous solution and then combine it with a particular solution for this non-homogeneous equation. So it is possible to write:

$$V^\pm(z, \Omega) = V^\pm(z_j, \Omega) e^{\pm j \frac{\Omega}{v_{g0}} (z-z_j)} e^{\pm \int_{z_j}^z \kappa(z', \Omega) dz'} \cdot \left[ 1 + \int_{z_j}^z F^\pm(z', \Omega) e^{\mp j \frac{\Omega}{v_{g0}} (z'-z_j)} e^{\mp \int_{z_j}^{z'} \kappa(z'', \Omega) dz''} dz' \right]$$

where  $z_j$  is a fixed spatial coordinate. By discretizing the longitudinal coordinate  $z$ , the mode amplitude can be written as:

$$\begin{aligned} V^\pm(z_{j\pm}, \Delta z, \Omega) &\simeq V^\pm(z_j, \Omega) e^{\pm j \frac{\Omega}{v_{g0}} \Delta z} e^{\kappa(z_j, \Omega) \Delta z} + F^\pm(z_j, \Omega) \Delta z = \\ &= F^\pm(z_j, \Omega) \Delta z + V^\pm(z_j, \Omega) e^{\pm j \frac{\Omega}{v_{g0}} \Delta z} \exp \left[ -\frac{\alpha_i}{2} \Delta z + \right. \\ &\quad \left. \Gamma_{xy} \sum_{i=1}^N \sum_{k=GS,ES_1,ES_2} \frac{1}{2} g_{0,k}^i (2\tilde{f}_k^i(z, \Omega) - 1) \otimes \mathcal{L}_k^i(\Omega) \Delta z \right] \\ &\simeq F^\pm(z_j, \Omega) \Delta z + V^\pm(z_j, \Omega) e^{\pm j \frac{\Omega}{v_{g0}} \Delta z} \left[ 1 - \frac{\alpha_i}{2} \Delta z + \right. \\ &\quad \left. \Gamma_{xy} \sum_{i=1}^N \sum_{k=GS,ES_1,ES_2} \frac{1}{2} g_{0,k}^i (2\tilde{f}_k^i(z, \Omega) - 1) \otimes \mathcal{L}_k^i(\Omega) \Delta z \right] \end{aligned}$$

by defining a time step  $\Delta t$  as  $\Delta t = \frac{\Delta z}{v_{g0}}$  the equation can be written in the time domain as:

$$V^\pm(z_j \pm \Delta z, t) = F^\pm(z_j, t)\Delta z + \left[ V^\pm(z_j, t - \Delta t) - \frac{\alpha_i}{2} V^\pm(z_j, t - \Delta t)\Delta z + \Gamma_{xy} \sum_{i=1}^N \sum_{k=GS,ES_1,ES_2} \frac{1}{2} g_{0,k}^i \left( 2\tilde{f}_k^i(z_j, t - \Delta t) - 1 \right) I_k^{\pm,i}(z_j, t - \Delta t)\Delta z \right] \quad (3.6)$$

where  $I_k^{\pm,i}(z_j, t) = \mathcal{L}_k^i \otimes V^\pm(z_j, t)$ . The field at each time step can be computed from its values in the previous time step by computing the values of  $I_k^{\pm,i}(z_j, t)$ , which represents the field (both forward and backward) filtered by the lorentzian filters. From 2.34, it is possible to write:

$$I_k^{\pm,i}(z_j, t) = e^{j(\omega_k^i - \omega_0)\Delta t} e^{-\Gamma\Delta t} I_k^{\pm,i}(z_j, t - \Delta t) + \frac{1}{2} \Gamma \Delta t e^{j(\omega_k^i - \omega_0)\Delta t} e^{-\Gamma\Delta t} V^\pm(z_j, t - \Delta t) + \frac{1}{2} \Gamma \Delta t V^\pm(z_j, t) \quad (3.7)$$

this allows to evaluate the convolution integral at a defined time step from the mode amplitude and its value in the previous time step. From this the stimulated emission rate can be derived as:

$$R_{st,k}^i(z_j, t) = \frac{\Gamma_{xy}}{\hbar\omega_0} g_{0,k}^i \left( 2\tilde{f}_k^i(z_j, t) - 1 \right) \cdot \text{Re} \left\{ V^+(z_j, t) I_k^{\pm,i*}(z_j, t) + V^-(z_j, t) I_k^{\pm,i*}(z_j, t) \right\} \quad (3.8)$$

## 3.2 Numerical modelling of the spontaneous emission noise

The spontaneous emission noise can be easily modeled due to its random nature. In each slice of the waveguide there has to be zero correlation with all the other slices, thus a set of random processes  $\varphi_k^{\pm,i}(z_j, t)$  can be used, having a uniform distribution between 0 and  $2\pi$ . This can be obtained by using a pseudo-random number generator. The field can be written as:

$$F^\pm(z_j, t)\Delta z = \sum_{i=1}^N \sum_k \sqrt{\frac{\beta_{sp} \hbar \omega_0 v_{g0} n_k^i(z_j, t)}{2\pi \Gamma \tau_{sp}}} I_{sp,k}^{\pm,i}(z_j, t) \quad (3.9)$$

and  $I_{sp,k}^{\pm,i}(z_j, t)$  can be evaluated in the same fashion as  $I_k^{\pm,i}(z_j, t)$ :

$$I_{sp,k}^{\pm,i}(z_j, t) = e^{j(\omega_k^i - \omega_0)\Delta t} e^{-\Gamma\Delta t} \left( I_{sp,k}^{\pm,i}(z_j, t - \Delta t) + \frac{1}{2} \Gamma \Delta t e^{j\varphi_k^{\pm,i}(z_j, t - \Delta t)} \right) + \frac{1}{2} \Gamma \Delta t e^{j\varphi_k^{\pm,i}(z_j, t)} \quad (3.10)$$

### 3.3 Summary

Having defined the numerical details, in this section the overall procedure is reported. At the beginning of the simulation a unit time step  $\Delta t$  is defined; this directly determines the longitudinal discretization  $\Delta z$  as  $\Delta z = \Delta t \times v_{g0}$ , defining the device structure. At this point the model variables are initialized and the following steps are iteratively repeated:

- Rate equations are solved in each slice thanks to the finite difference approach, obtaining the occupation probabilities of each QD state
- The convolution integrals are evaluated from 3.7 and 3.10
- The spontaneous emission noise is generated thanks to 3.9
- The overall forward and backward components of the field at the subsequent time step are computed in each slice by means of 3.6

# Chapter 4

## Model implementation

In this chapter the physical parameters used in the simulations of the device are presented, along with a specific implementation of an external feedback mechanism needed for the simulation of the double pass configuration presented in Fig. 1.2. The code implementations can be observed in Appendix A. The composition of the active region of the amplifier is shown in Fig. 4.1. The epitaxial structure is composed by three different types of QD, each of them with a specific number of layers associated. Starting from the p-contact a group of 3 layers with GS emission of 1211nm is found, followed by another triplet of layers with a central emission of 1243nm; lastly, at the n-contact, a four-layer group with central GS emission of 1285nm is found. Each layer belonging to a group of QD is supposed as identical to the other layers of the same group, thus allowing to define the characteristic of only a single layer of each set and then replicating its

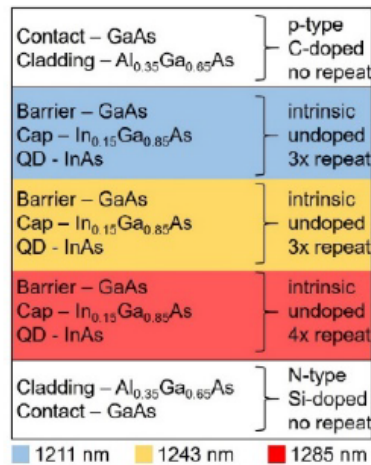


**Figure 4.1:** Schematic representation of the epitaxial structure, courtesy of [5]

definition. The tapered shape of the device is implemented by assigning to each slice  $z$  a different width, following the schema below:

$$\begin{cases} w(z) = 14\mu m & z < 500\mu m \\ w(z) = 14\mu m + 2 * (z - 500\mu m)tg(\frac{3^\circ}{2}) & 500\mu m < z < 1000\mu m \\ w(z) = 14\mu m + 2 * (500\mu m)tg(\frac{3^\circ}{2}) + 2 * (z - 1000\mu m)tg(\frac{0.8^\circ}{2}) & z > 1000\mu m \end{cases}$$

One thing that must be noticed is the fact that in the developed code the optical power is injected from  $z = 0$ , thus in the double pass setup this description has to be reversed, putting the front section at  $z = 0$ . This is simply done by defining the structure using the same schema, and then flipping it thanks to the MATLAB command `flip(z)`. A key feature of the double pass configuration is the external feedback mechanism: the signal after being emitted from the rear section travels for an additional 1 mm in air; after this free flight, the amplified signal is reflected by a mirror to be amplified again by the SOA during a second pass. This was implemented thanks to two circular buffers, one that describes the travelling of the field before the reflection of the external mirror and one describes the travelling of the optical field after the reflection. The last difference that has to be taken into account when comparing the single pass and the double pass configuration is the fact that the propagation losses ( $\alpha$ ), introduced in 2.11 are different when the field travels from the front section to the rear one and vice versa, for this reason two different values are assigned to this parameter.

## 4.1 Reference frequency and time step

In the description of the model, since the introduction of the slowly varying envelope approach, a reference frequency  $\omega_0$  has been defined. This parameter must be carefully picked since it must guarantee the validity of the aforementioned approximation. Moreover is necessary to define a reference frequency that allows to properly resolve the interband transitions of the confined states. In the developed code the reference frequency is evaluated from the reference energy. Three choices are available:

- GS: the reference energy is chosen as the average between the GS transition energies;
- ES1: the reference energy is chosen as the average between the GS and ES1 transition energies;
- ES2: the reference energy is chosen as the average between the GS and ES2 transition energies;

Thanks to experimental results previously obtained for this device ([6, 5]) it was possible to choose a priori the reference energy as the average between the GS and ES1 transition energies, being these the two main contributions to the stimulated emission. Having chosen the reference frequency the time step  $\Delta t$  is chosen in order to avoid aliasing by

ensuring that the central frequency of the Lorentzian filters  $\omega_k^i - \omega_0$  is much smaller than the Nyquist frequency  $\frac{\pi}{\Delta t}$ . A lower bound of this simulation step is given by the computation time and by the limited numerical precision of the simulating system. For these reasons a time step of 15 fs was chosen.

## 4.2 Physical parameters

The main parameters used in the simulations are reported in 4.1: Having defined

Symbol	Meaning	Value
$n_l$	Number of quantum dot layers	4,3,3
$E_{GS}^l$	Interband transition for GS	1.0239-0.9976-0.9650 eV
$E_{ES1}^l$	Interband transition for ES1	1.0500-1.0265-0.9960 eV
$E_{ES2}^l$	Interband transition for ES2	1.0690-1.0508-1.0333 eV
$E_{WL}$	Wetting layer transition energy	1.1 eV
$g_i$	Maximum gain for GS, ES1 and ES2	690-750-700 $cm^{-1}$
$\alpha$	Propagation losses	1.35 (R $\rightarrow$ F), 3.60 (F $\rightarrow$ R) $cm^{-1}$
$K_p$	Plasma losses coefficient	$10^{-17} cm^2$
$\tau_{c,i}$	Capture times from ES1, ES2 and WL	5-5-12 ps
$\tau_{nr,i}$	Non-radiative times	10 ns
$\tau_{A,i}$	Auger times for GS, ES1, ES2	0.44-2.2-3.3 ns
$\eta$	Injection efficiency	0.65

**Table 4.1:** Physical parameters

everything needed for the numerical implementation of the model, in the next two chapters simulation results are presented.

## Chapter 5

# Tunable spectral asymmetry

The output characteristics of tapered devices has been acquired and analyzed in several conditions ([25]), in this chapter, by using the developed model, will be shown the tunable spectral asymmetry of the aforementioned device. In order to do so, apart from previously discussed parameters, it must be noticed that the device is simulated without any kind of feedback mechanism (meaning that no reflectivity is imposed on both the rear and the front facet).

The analysis will mainly focus on two specific conditions:

1.  $I_R = 0.1A$   $I_F = 1A$
2.  $I_R = 0.1A$   $I_F = 3.5A$

One of the key values to look during the analysis is the occupation probability of both the rear and front sections, since, by implementation, the gain has a direct relation with them:

```
GainES2(:, :, pp)=0.5*(GainES2_mod.*(RhocbES2+RhovbES2-1)-DalfaiES2);  
GainES1(:, :, pp)=0.5*(GainES1_mod.*(RhocbES1+RhovbES1-1)-DalfaiES1);  
GainGS(:, :, pp)=0.5*(GainGS_mod.*(RhocbGS+RhovbGS-1))./(1+GainCompressionGS);
```

thus, before considering losses, the values of the occupation probabilities will have a direct impact on the gain spectra. For the first setup the obtained occupation probabilities are reported in 5.2 and 5.1, a graphical depiction of the two is shown in Fig. 5.1.

	GS	ES1	ES2
G1	0.85	0.51	0.18
G2	0.67	0.22	0.07
G3	0.57	0.09	0.01

**Table 5.1:** Occupation probability of the 3 considered QD groups in the rear section for the 0.1/1 A setup.

	GS	ES1	ES2
G1	0.90	0.53	0.23
G2	0.74	0.24	0.08
G3	0.60	0.10	0.01

**Table 5.2:** Occupation probability of the 3 considered QD groups in the front section for the 0.1/1 A setup.

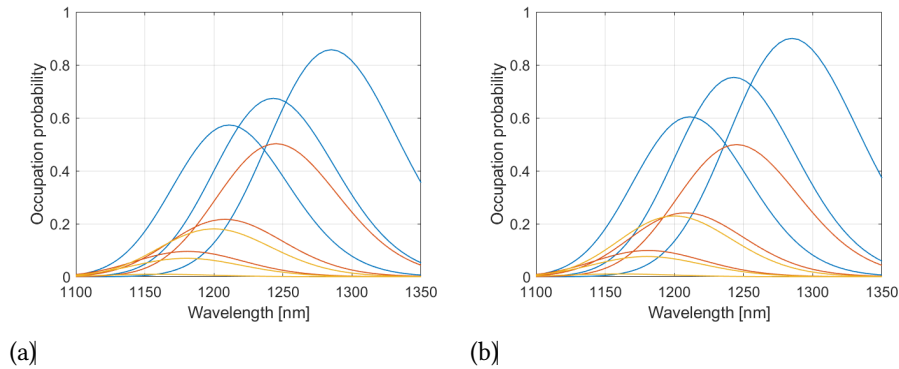


**Figure 5.1:** Occupation probability in the rear (a) and front (b) section for the 0.1/1 A setup

What can be noticed is the similarity in occupation probability between the two. Due to the low injected current only the GS can ensure values that allow for an actual optical amplification. By looking at both gain spectra reported in Fig. 5.2, it can be noticed how the absorption induced by the excited states allows for a positive peak only around the 1270nm wavelength, and an overall low gain for wavelengths above 1250nm. This shape is coherent with the simulation results obtained in [5] and reported in Fig. 5.3. In Fig. 5.4 the output spectra from both facets have been plotted and normalized with respect to one another, in order to properly show the relative difference between the two.

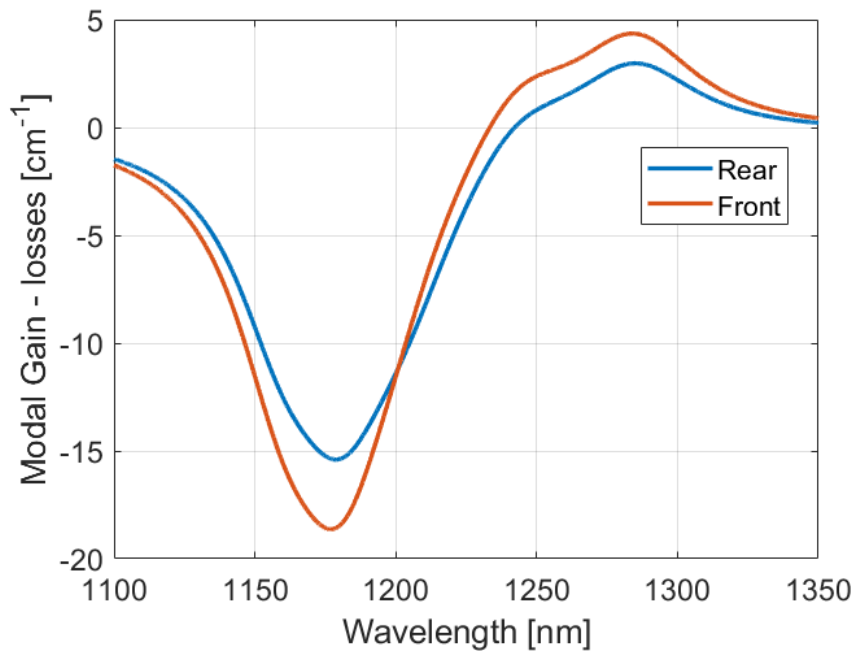


**Figure 5.2:** Gain spectra in the rear and front section for the 0.1/1 A setup

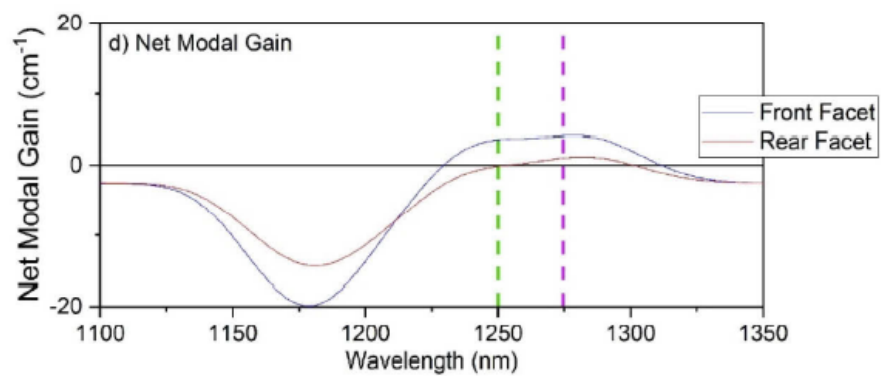


**Figure 5.3:** Simulation results for the 0.1/1 A setup, courtesy of [5]

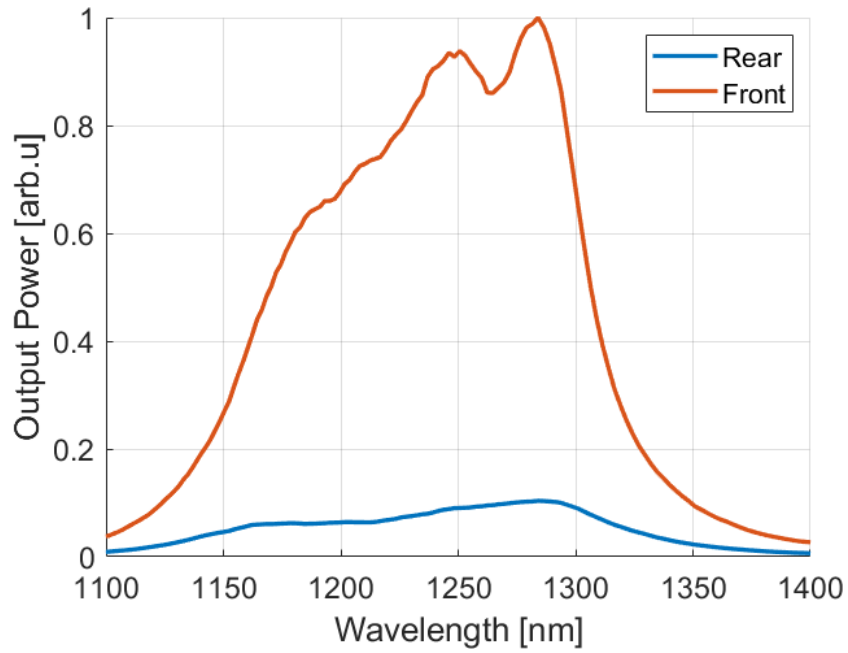


**Figure 5.4:** Output spectra in the rear and front section for the 0.1/1 A setup

The effects of the aforementioned gain spectra are clearly visible, with peaks in correspondence of the Ground States with an occupation probability that allow for an actual gain.

The values of the occupation probabilities for the second setup are reported in 5.3 and 5.4, and shown in Fig. 5.5. The effect of the higher injection current can be clearly noticed on the front section, where all the GS have an occupation probability close to 1 and several excited states now contribute to the gain, that can be observed in Fig. 5.6.

	GS	ES1	ES2
G1	0.77	0.48	0.18
G2	0.69	0.21	0.07
G3	0.45	0.09	0.01

**Table 5.3:** Occupation probability of the 3 considered QD groups in the rear section for the 0.1/3.5 A setup.

	GS	ES1	ES2
G1	0.96	0.87	0.68
G2	0.98	0.78	0.48
G3	0.95	0.60	0.25

**Table 5.4:** Occupation probability of the 3 considered QD groups in the front section for the 0.1/3.5 A setup.

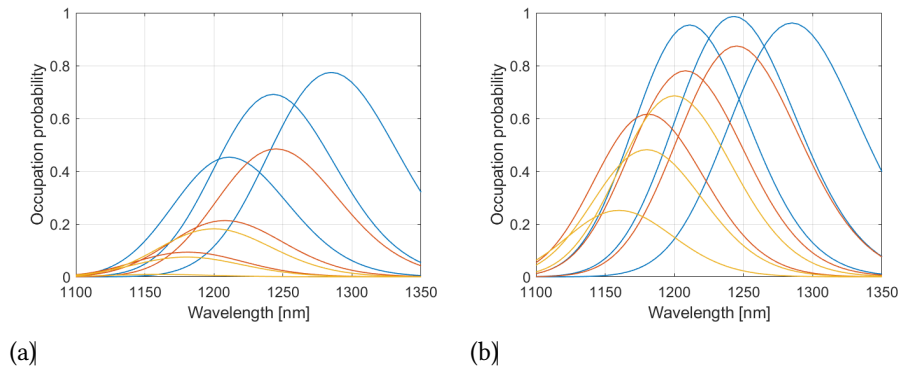


**Figure 5.5:** Occupation probability in the rear (a) and front (b) section for the 0.1/3.5 A setup

Also for this setup the gain spectra obtained with the developed TDTW model are in agreement with the results of [5], reported in Fig. 5.7

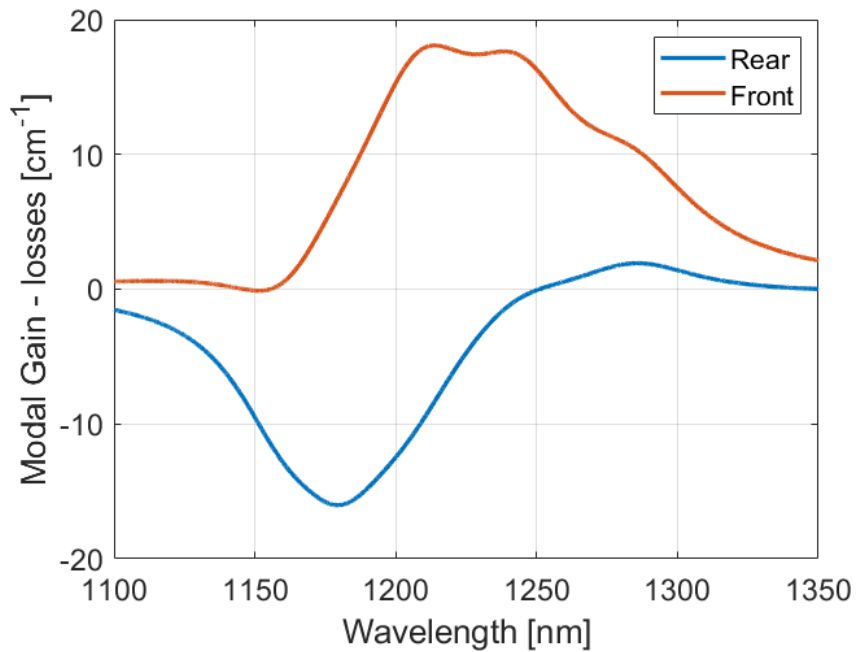


**Figure 5.6:** Gain spectra in the rear and front section for the 0.1/3.5 A setup

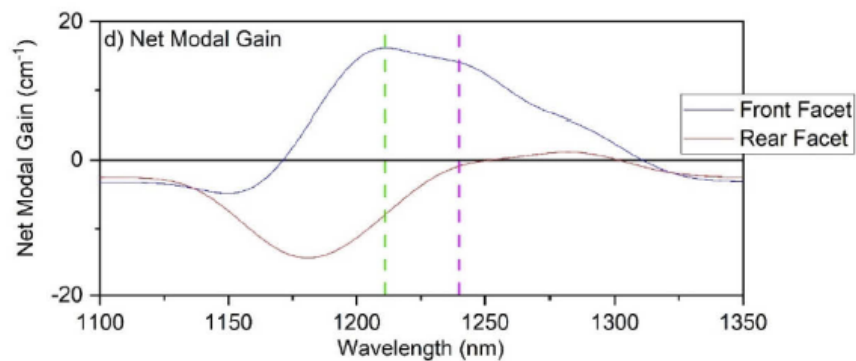


**Figure 5.7:** Simulation results for the 0.1/3.5 A setup, courtesy of [5]

In the output spectra reported in Fig. 5.8 the influence of the gain asymmetry is clear: in the front section two peaks can be observed around the 1240nm and 1210nm wavelengths, where the majority of the states that contribute to the gain are present, namely the GS for the second and third group, and the first excited states for the first and second group of QDs.

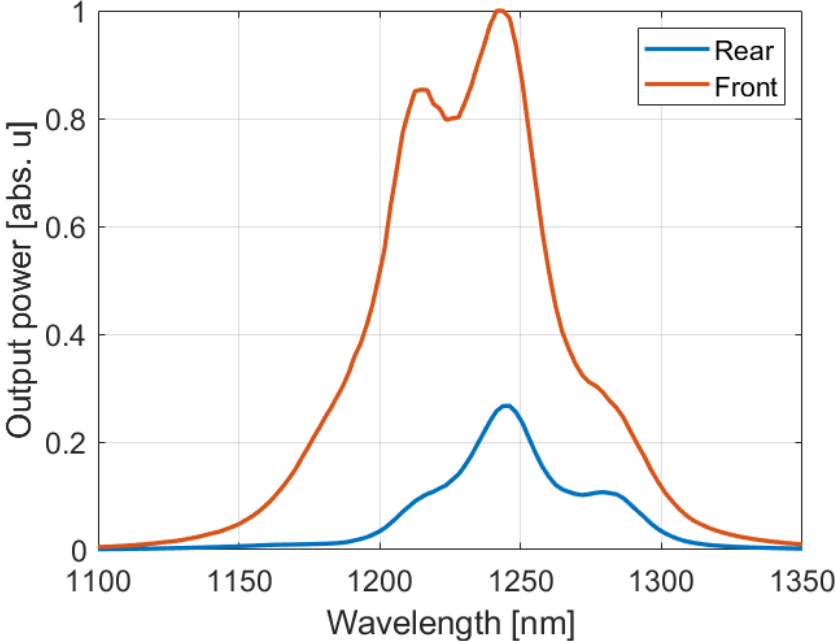
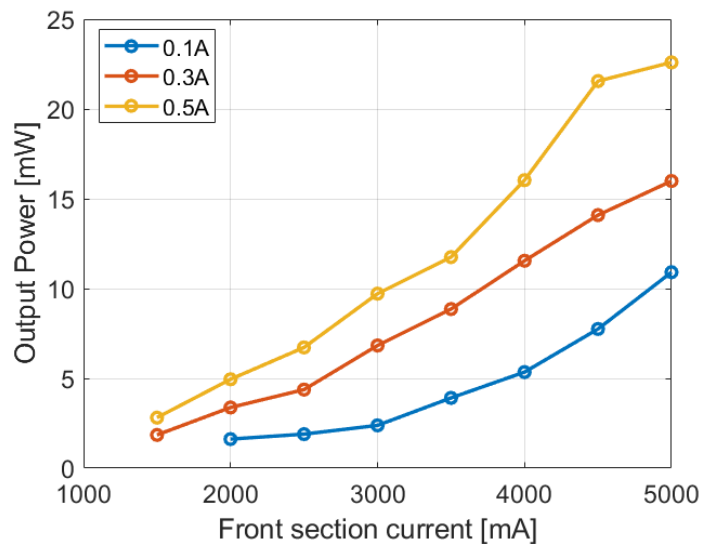


Figure 5.8: Output spectra in the rear and front section for the 0.1/3.5 A setup

## Chapter 6

# Double-Pass amplification

In this chapter the comparison between the single-pass and the double-pass configuration is reported. At first the Single Pass configuration was simulated, with an input power of 1 mW. The simulations are performed in the following conditions: rear section current of [0.1 A, 0.3 A, 0.5 A] and front section current of [1.5 A, 2 A, 2.5 A, 3 A, 3.5 A, 4 A, 4.5 A, 5 A]. For the 0.1 A/1.5 A configuration results are not shown since losses overcame the gain, showing no particular behaviour of interest.



**Figure 6.1:** Output power for the single pass configuration

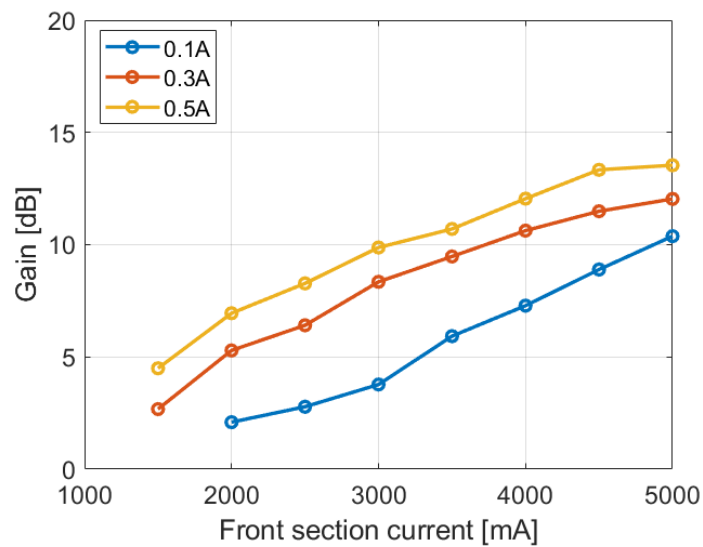


**Figure 6.2:** Gain for the single pass configuration

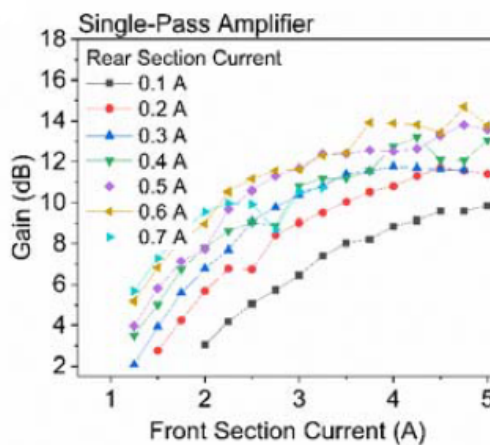


**Figure 6.3:** Experimental gain for the single pass configuration, courtesy of [6]

The increase in rear section current directly influences its gain profile, thus increasing the output power. The gain values are in good agreement with the experimental results of [6], reported in Fig. 6.3, thus proving the validity of the model for the single-pass configuration.

Results for the double pass configuration can be observed in Figs 6.4 and 6.5. The setup conditions for the 0.1 A front section current configuration replicates the one of the single pass configuration to allow for a clear comparison, while higher front section

current configurations ([0.3 A,0.5 A]) are simulated at lower front section currents.

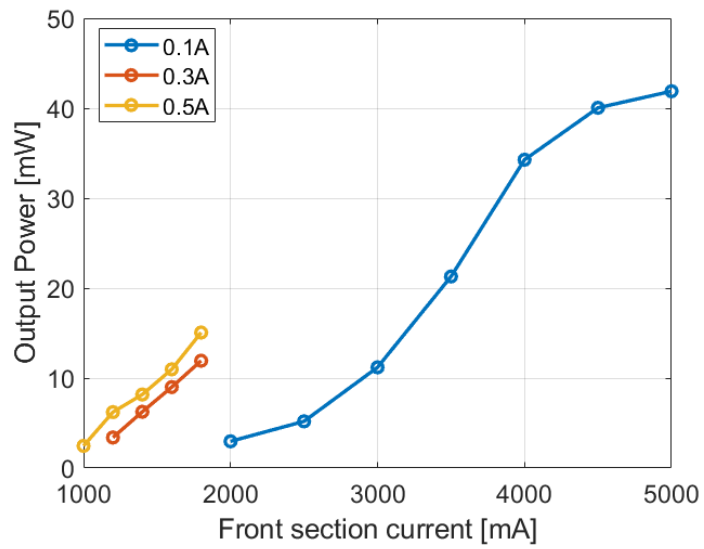


Figure 6.4: Output power for the double pass configuration

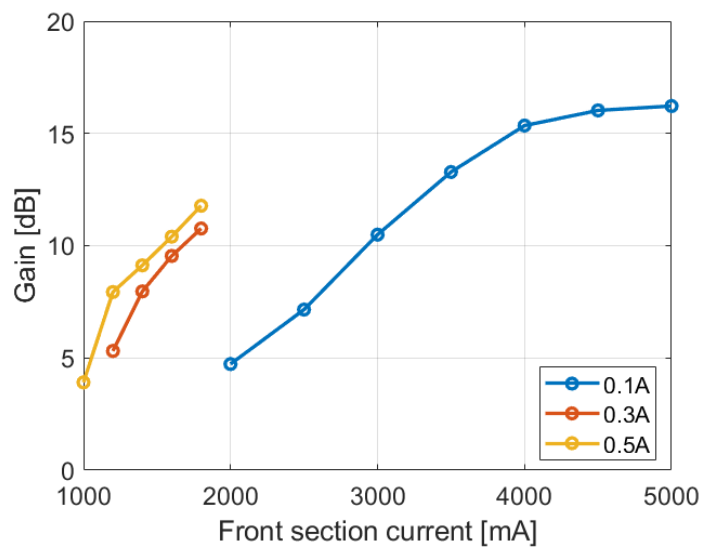
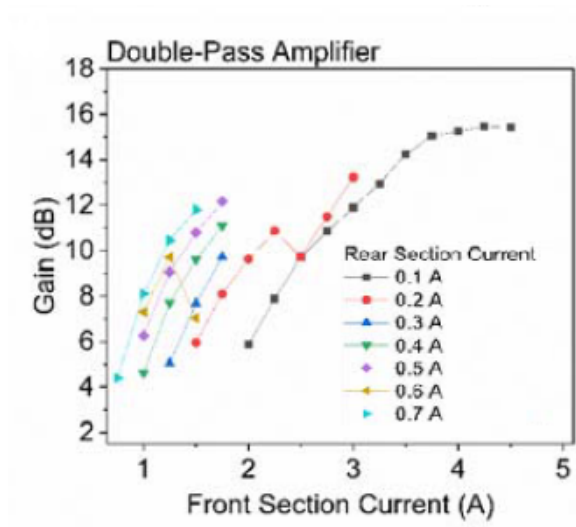
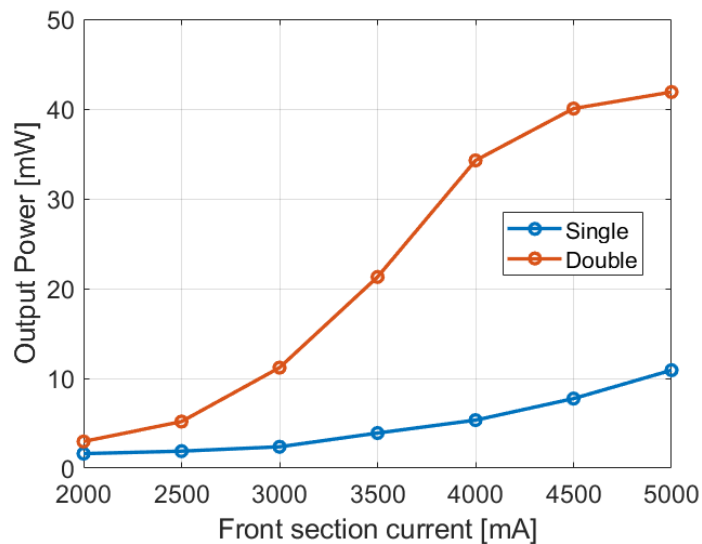


Figure 6.5: Gain for the double pass configuration



**Figure 6.6:** Experimental gain for the double pass configuration, courtesy of [6]

Once again the gain values are in good agreement with the experimental results of [6], reported in Fig. 6.6. In Figs. 6.7 and 6.8 the comparison between the two configurations can be observed. The double pass configuration provides, as expected, an higher output power, mainly due to the fact that the signal has to pass through the active region twice, and even though the signal must sustain more losses, especially due to the fact that in the round trip it has to go from the front section to the rear one first, in the double pass configuration we can clearly observe a higher gain.



**Figure 6.7:** Output power for both configurations at fixed rear current of 0.1A

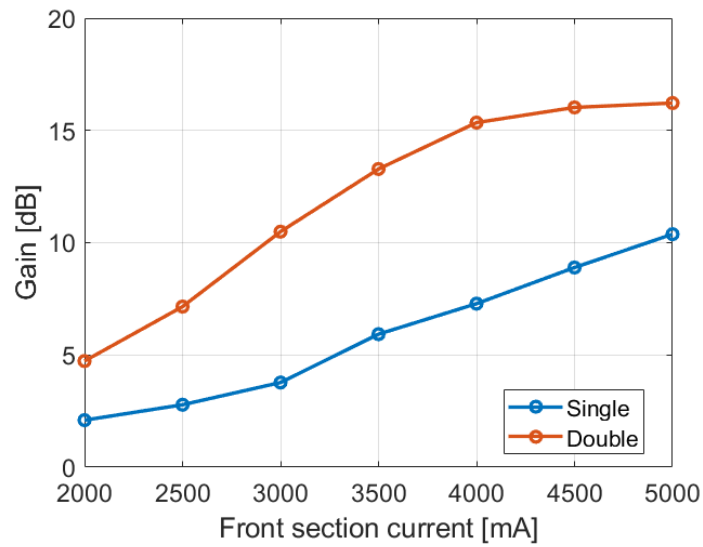


**Figure 6.8:** Gain for both configurations at fixed rear current of 0.1A

Between the two configurations in the same conditions a steady gain difference of at least 2.6 dB can be observed with a peak difference of approximately 8 dB at the 0.1 A/4 A rear/front section current point. At higher currents the gain in the double pass configurations starts to flatten, leading to lower gain differences. Further proofs of the effects of the active region can be observed in Fig. 6.9, in which are plotted the output spectra for both the single and double pass configurations. Both output spectra have been normalized in order to allow for a spectral comparison between the two. While all of them present a peak around the 1240nm wavelength, the difference between the two configurations can be observed by looking at the 1210nm peak, where in every simulation the double pass configuration shows an higher peak. This is due to the fact that the 1210nm peak, as shown in Fig. 5.6 is influenced by the gain profile of the front section when an high enough injection current is injected.

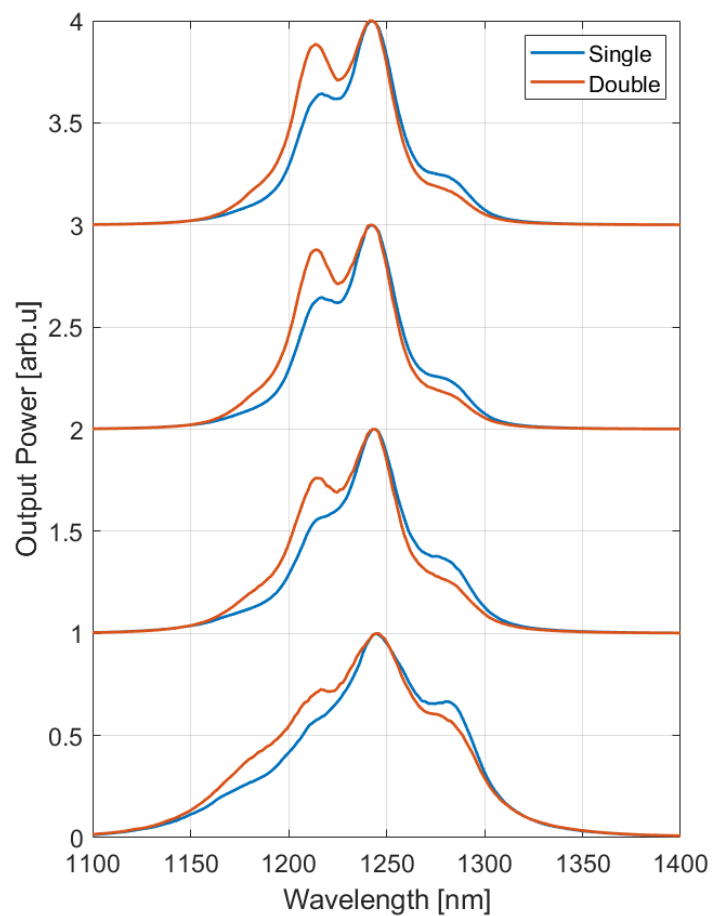


**Figure 6.9:** Output power spectra of both configurations at increasing front current

The obtained results are in good agreement with the experimental ones obtained for this device, showing both the high tunability that can be obtained with the implementation of two electrodes, and showing the undoubtable advantages of the double pass configuration with respect to the single pass one, providing a cheap and efficient technique to improve the optical gain of the SOA.

## Chapter 7

# Conclusions

In this work the modeling of chirped quantum dot based optoelectronic devices has been developed by working on an existing TDTW model. To allow for reasonable simulation time, all the QDs with central GS emission at the same wavelength were regrouped, and the different groups were weighted according to number of similar active layers.

Simulation results were compared with simulations obtained with different models, showing an high level of fidelity, while also presenting the limitations induced by the use of a single population approach, mainly in the presence of too well defined emission peaks. Moreover, thanks to a collaboration with the Institute of Photonics and Quantum Sciences of the Heriot-Watt University in Edinburgh, simulation results for the single and double pass amplification configuration have been compared with their experimental counterparts. In this framework simulation results were in good agreement with the experimental ones, showing a discrepancy of no more than 10%, being able to replicate the measured advantages of the double pass configuration.

Multi-population approaches have been developed for this model, but due to their high computational times they have not been tested against experimental results. For simplicity similar states of different groups are treated as a unique set in all the implementations (all GS are accessible by all ES1, and similar), thus further development of this model could include a three dimensional treatment in which the states of a group are only capable of interacting with states of the same group.

# Appendix A

## Code implementations

In this appendix all of the implementations made for this work are shown and discussed, along with other solutions that have been implemented but not used to obtain the results of Chapters 5 and 6.

### A.1 Modelling chirped QD

When modeling an ensemble of self-assembled quantum dots the following distribution has been defined to properly take into account the variance of the growth process:

$$G_i = 1/Z \exp\left(-4 \log 2 \frac{\hbar\omega_{i,GS} - \hbar\omega_{(N+1)/2,GS}}{\Delta E^2}\right) \quad (\text{A.1})$$

In order to properly model chirped quantum dots, since in the implemented model all the characteristic interband transition energies for the QD populations belong to one vector depending on the state (one vector for the GS, one for ES1, and so on) three different solutions have been implemented. Starting from the characteristic interband transition energy (expressed in eV):

```
1 EnergyGapQDCentralPop = [...  
2   1.0690, 1.0508, 1.0333;  
3   1.0500, 1.0265, 0.9960;  
4   1.0239, 0.9976, 0.9650  
5   ];
```

the main objective is to obtain the distribution of the existence probability of each QD population. The previous implementation, that works only if one group of QD has to be simulated, is hereby reported:

**Listing A.1:** Previously developed distribution of the existence probability of each QD population

```

1 % [1,1] (Always odd) number of QD population created in EnergyGapQD []
2 NumQDPopulations = 51;
3 % [NumStates,1] FWHM->sigma of inhomogeneous broadening of the QD
   ensemble (ES2, ES1, GS) [eV]
4 InhomDeltaE = [0.035;0.035;0.035]/sqrt(8*log(2));
5 % [NumStates,NumPops] Characteristic interband transition energies for
   the QD populations (ES2; ES1; GS) [eV]
6 EnergyGapQD = [...
7     linspace(EnergyGapQDCentralPop(1)+3*InhomDeltaE(1),
8     EnergyGapQDCentralPop(1)-3*InhomDeltaE(1),NumQDPopulations);
9     linspace(EnergyGapQDCentralPop(2)+3*InhomDeltaE(2),
10    EnergyGapQDCentralPop(2)-3*InhomDeltaE(2),NumQDPopulations);
11    linspace(EnergyGapQDCentralPop(3)+3*InhomDeltaE(3),
12    EnergyGapQDCentralPop(3)-3*InhomDeltaE(3),NumQDPopulations);
13 ];
14 % [NumStates,NumPops] Gaussian distribution of the existence prob. of
   each QD population [>=0]
15 Inhomog_distribution = ...
16     exp(-(EnergyGapQD-repmat(EnergyGapQDCentralPop,1,NumQDPopulations
17     )).^2./(2*repmat(InhomDeltaE,1,NumQDPopulations).^2));
18 % [NumStates,NumPops] Normalized distribution of the existence prob.
   of each QD population. The sum (per rows) is 1 [>=0]
19 Inhomog_distribution = ...
20     Inhomog_distribution ./ repmat(sum(Inhomog_distribution,2),1,
21     NumQDPopulations);

```

But this implementation does not guarantee a valid method for modelling chirped quantum dots. The first solution that one could use is to consider only one population per QD group, thus defining it in the following way:

**Listing A.2:** Single population approach

```

1 % [NumStates,NumPops] Characteristic interband transition energies for
   the QD populations (ES2; ES1; GS) [eV]
2 EnergyGapQD=EnergyGapQDCentralPop;
3 %Factor that takes into account the weight of different QD groups
4 Mult = [4,3,3];
5 %Number of QD groups
6 NumDiffDots = size(EnergyGapQDCentralPop,2);
7 % [NumStates,NumPops] Distribution of the existence prob. of each QD
   population [>=0]
8 Inhomog_distribution = zeros(3,NumDiffDots);
9 for ii = 1:NumDiffDots
10     Inhomog_distribution(:,ii) = Mult(ii);
11 end
12 % [NumStates,NumPops] Normalized distribution of the existence prob.
   of each QD population. The sum (per rows) is 1 [>=0]

```

```

13 Inhomog_distribution = ...
14   Inhomog_distribution ./ repmat(sum(Inhomog_distribution , 2) , 1 ,
    NumQDPopulations);

```

This represents the easiest solution, and also the one that requires less computational time between all of them, since only one population per energy state per group is considered. The other two implemented solutions keep the Gaussian distribution of the first implementation and rely on the following definition of the Characteristic interband transition energies for the QD populations:

**Listing A.3:** Multiple populations definition of the Characteristic interband transition energies

```

1 function EGQD = FuncEnergyGapQD (EnergyGapQDCentralPop , InhomDeltaE ,
    NumLevPop , NumDiffDots)
2 EGQD = [];
3 dist = abs ( diff ( EnergyGapQDCentralPop ' ) ) / 2 * 0.98;
4
5 for ii = 1:NumDiffDots
6     if ii == NumDiffDots
7         Lim = dist ( ii - 1 , : );
8     elseif ii == 1
9         Lim = dist ( 1 , : );
10    else
11        Lim = min ( dist ( ii , : ) , dist ( ii - 1 , : ) );
12    end
13
14    vec = [ ...
15        linspace ( EnergyGapQDCentralPop ( 1 , ii ) + Lim ( 1 ) ,
    EnergyGapQDCentralPop ( 1 , ii ) - Lim ( 1 ) , NumLevPop );
16        linspace ( EnergyGapQDCentralPop ( 2 , ii ) + Lim ( 2 ) ,
    EnergyGapQDCentralPop ( 2 , ii ) - Lim ( 2 ) , NumLevPop );
17        linspace ( EnergyGapQDCentralPop ( 3 , ii ) + Lim ( 3 ) ,
    EnergyGapQDCentralPop ( 3 , ii ) - Lim ( 3 ) , NumLevPop );
18        ];
19
20    EGQD = [EGQD vec];
21
22 end
23 upExt = [ ...
24     linspace ( EnergyGapQDCentralPop ( 1 , 1 ) + 3 * InhomDeltaE ( 1 ) , EGQD ( 1 , 1 ) ,
    NumLevPop + 1 );
25     linspace ( EnergyGapQDCentralPop ( 2 , 1 ) + 3 * InhomDeltaE ( 2 ) , EGQD ( 2 , 1 ) ,
    NumLevPop + 1 );
26     linspace ( EnergyGapQDCentralPop ( 3 , 1 ) + 3 * InhomDeltaE ( 3 ) , EGQD ( 3 , 1 ) ,
    NumLevPop + 1 );
27     ];
28 upExt = upExt ( : , 1 : end - 1 );
29

```

```

30 dwExt = [ ...
31     linspace(EGQD(1, end), EnergyGapQDCentralPop(1, end) - 3*InhomDeltaE
32     (1), NumLevPop+1);
32     linspace(EGQD(2, end), EnergyGapQDCentralPop(2, end) - 3*InhomDeltaE
33     (2), NumLevPop+1);
33     linspace(EGQD(3, end), EnergyGapQDCentralPop(3, end) - 3*InhomDeltaE
34     (3), NumLevPop+1);
34 ];
35 dwExt = dwExt(:, 2:end);
36 EGQD = [upExt EGQD dwExt];
37 end

```

What the previous code does is to at first evaluate the distances (`dist`) between the energy levels, reduces it to 98% of their value in order to avoid the overlap between two neighbour, then, using half the distances, creates symmetrical intervals across each transition energy with a defined number of populations (`NumLevPop`) equal for all the transition energies and merges them. Lastly, to take into account the tails of the Gaussian distribution, two extensions are added. Having defined the vector of transition energies, the distribution of the existence probability can be defined in two different manners, depending on the use case:

#### Listing A.4: Approach 1 for the distribution of the existence probability

```

1 function ID = FuncInhomg_distribution(EnergyGapQDCentralPop ,
2   InhomDeltaE , EnergyGapQD , NumQDPop, NumDiffDots , Mult)
3 ID = zeros(3, NumQDPop);
4 for ii = 1:NumDiffDots
5     vec = Mult(ii) * exp(-(EnergyGapQD - repmat(EnergyGapQDCentralPop(:,
6     ii), 1, NumQDPop)).^2 ./ (2 * repmat(InhomDeltaE, 1, NumQDPop).^2));
7     ID = ID + vec;
8 end
9 end

```

With this approach the a Gaussian distribution for each transition energy is defined and added together per state. The resulting distribution can be observed in Fig. A.1:

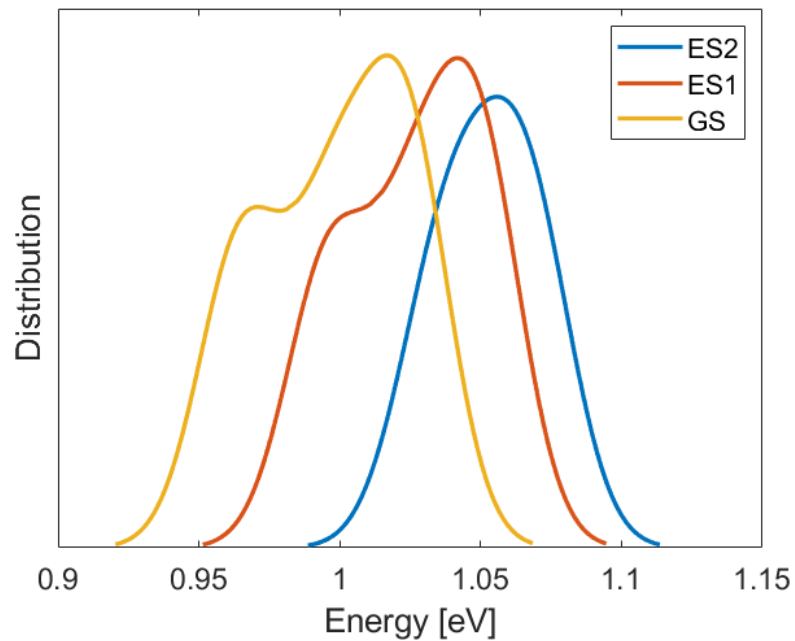


**Figure A.1:** Distribution of the existence probability obtained with A.4

This approach correctly defines the distribution for each quantum dot group, but when all of them are added together, the uniqueness of each quantum dot is lost. For this reason the third solution has been developed:

**Listing A.5:** Approach 1 for the distribution of the existence probability

```

1 function ID = FuncInhomg_distribution(EnergyGapQDCentralPop ,
2   InhomDeltaE , EnergyGapQD , NumDiffDots , Mult , NumLevPop)
3
4 for ii = 1:NumDiffDots
5     if ii == 1
6         NumPops = 2*NumLevPop;
7         stIdx = 1;
8     elseif ii == NumDiffDots
9         NumPops = 2*NumLevPop;
10        stIdx = (ii)*NumLevPop+1;
11    else
12        NumPops = NumLevPop;
13        stIdx = (ii)*NumLevPop+1;
14    end
15
16    enIdx = stIdx+NumPops-1;

```

```

17     vec = Mult(ii) * exp(-(EnergyGapQD(:, stIdx:enIdx) - repmat(
    EnergyGapQDCentralPop(:, ii), 1, NumPops)).^2 ./ (2 * repmat(InhomDeltaE
    , 1, NumPops).^2));
18     ID = [ID vec];
19 end
20 end

```

This function defines a Gaussian distribution for each transition energy and assigns each distribution only to the segments on which that specific transition energy is defined. The overall distribution can be observed in Fig. A.2.

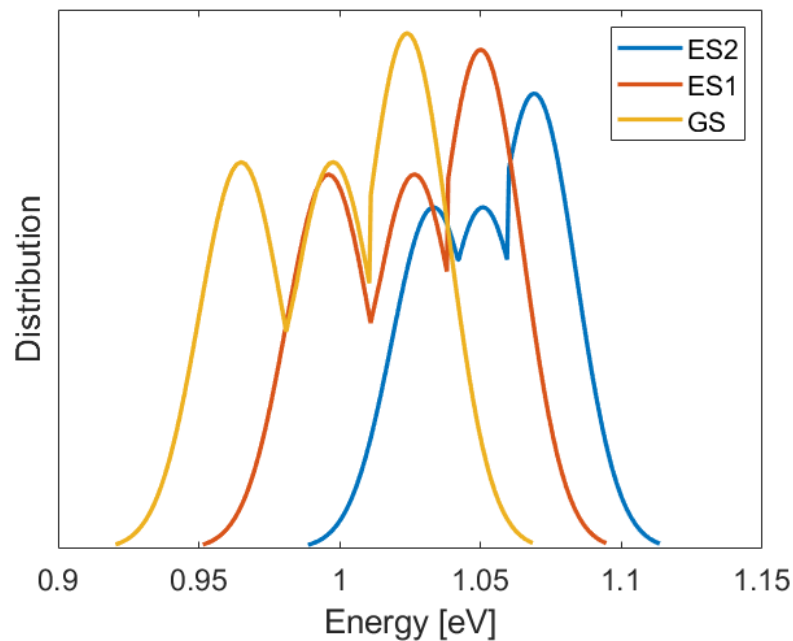


**Figure A.2:** Distribution of the existence probability obtained with A.5

With the latter approach the uniqueness of each quantum dot group is preserved. One thing that must be noticed is the fact that, by increasing the overall number of populations with these two implementations also the computational time is increased: for a simulation time of 40 ns the single population approach (3 populations per confined state) takes approximately 24 hours, while the multi-populations approaches the computational times reaches one week when considering 11 populations per level (55 populations per confined state).

## A.2 Modeling tapered structures

In order to model the tapered structure the following function has been defined:

```

1 function w=Width(z)
2 %Waveguide width as a function of the longitudinal position
3 %Input:
4 %   z: [1,NumSlices] slices positions [um]
5 %Output:
6 %   w: [1,NumSlices] waveguide widths [um]
7 % Internal inputs:
8 % - initial width: W0 [um]
9 % - tilt angle teta1 starting at length z1
10 % - tilt angle teta2 starting at length z2 (overriding teta1)
11 w = ones(size(z));
12 W0 = 14;
13 z1 = 500; z2 = 1000;
14 teta1 = 3 * pi/180; % [degree -> rad]
15 teta2 = 0.8 * pi/180; % [degree -> rad]
16 w(z<z1) = W0;
17 w(z<z2 & z>=z1) = W0+2*(z(z<z2 & z>=z1)-z1)*tan(teta1/2);
18 w(z>=z2) = W0+2*(z2-z1)*tan(teta1/2) + 2*(z(z>=z2)-z2)*tan(teta2/2);

```

With this parametric approach one could easily change structure as needed, and the introduction of subsequent tapered section could be easily implemented. The obtained width as a function of the longitudinal position  $z$  can be observed in Fig. A.3:

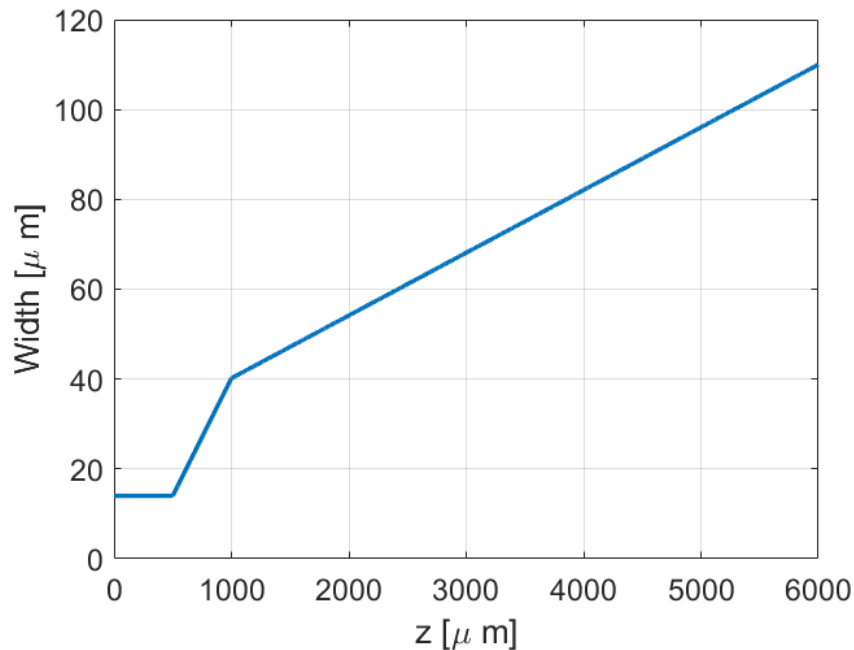


**Figure A.3:** Width as a function of the longitudinal position  $z$

### A.3 Modeling multiple electrodes

Since in the performed simulations it was needed to apply different injection currents in different regions of the device an Electrode index was assigned to each slice of the device. This code also allows to identify reversely polarized regions by assigning a negative index. Snippets of code used for the single pass configuration in the 0.1/3.5 A are reported in A.6

**Listing A.6:** Multi code electrode example

```

1 function E=Electrode(z)
2 E=ones(size(z));
3 f_e = @(z) 1+(z>1875);
4 E=f_e(z);
5 end
6
7 [...]
8
9 Sim.Pilot = @(e) 100*(e==1) + 3500*(e==2);
10
11 [...]
12
13 Pilot=Sim.Pilot(Electrode);

```

## A.4 Modeling the external feedback

The double circular buffer implementation for the external feedback mechanism is hereby reported. At first is necessary to define the characteristics of the feedback path:

```

1 Data.rF=1;
2 Data.LF=1000;

```

where  $rF$  represents the mirror feedback reflectivity and  $LF$  the length of the external feedback. Starting from this all the other parameters are evaluated and variables are allocated:

```

1 %[1,1] Field transmittivity of the external cavity [in modulus: >=0,
   <=1]
2 tF=sqrt(1-rF^2);
3 %[1,1] Number of slices in the external path [#]
4 NumSlicesF=2*floor(LF/dz);
5 %[1,NumSlicesF, COMPLEX] Field just before the reflection by the
   external mirror
6 EFeedback=AllocateComplex(1, NumSlicesF);
7 %[1,NumSlicesF, COMPLEX] Field just after the reflection by the
   external mirror
8 EFilteredFeedback=AllocateComplex(1, NumSlicesF);
9 %[1,1] position of the last item inserted in EFilteredfeedback and
   EFeedback [#]
10 kFeedback=int32(1);

```

Having defined all the variables, in the main time loop at each time step the progressive field  $S^+$  at  $z = L$  gets in part reflected and in part transmitted, being moved in the first buffer, while the field reflected by the external mirror is injected in the regressive field  $S^-$  of the device at  $z = L$ .

```

1 EFilteredFeedback(kFeedback)=...
2   EFeedback(kFeedback)*rF;
3 Sregr(pp, end)=Sregr(pp, end)+...
4   EFilteredFeedback(kFeedback)*FeedbackPropagationSingle*tL;
5 EFeedback(kFeedback)=(Sprog(pp, end)*tL+...
6   EFilteredFeedback(kFeedback)*FeedbackPropagationSingle*(-rL))*
7   FeedbackPropagationSingle;
8 if kFeedback==NumSlicesF
9   kFeedback=1;
10 else
11   kFeedback=kFeedback+1;

```

12 end

## A.5 Carriers variation

In this section the code that governs the carriers variation, reproducing the rate equations presented in chapter 2 are shown. For clarity the corresponding rate equations are reported. At first the variation of carriers in the separate confinement heterostructure are evaluated. In this, apart from the non radiative recombination process, present in every state, the capture and escape rates from the wetting layer have to be considered. Moreover if reversely biased regions were present, the tunneling from the confined states of these regions should be considered.

$$\frac{\partial n_{SCH}}{\partial t} = \eta_i \frac{J}{e} W - \frac{n_{SCH}}{\tau_{SCH \rightarrow WL}} + \frac{n_{WL}}{\tau_{WL \rightarrow SCH}} - \frac{B_{SCH}}{W \cdot h_{SCH}} n_{SCH}^2 - \frac{n_{SCH}}{\tau_{nr, SCH}} \quad (A.2)$$

```

1 %%%% Variation of SCH carriers in each slice in dt %%%%
2 %[1,NumSlices] Conversion coefficient from current [mA] to carriers
   in each slice [mA^-1 ns^-1]
3 NetCurrentCoeff=Data.Etai/1000/1e9.*FrazioneAreaElettrodi/Constants.e
   ;
4 %[1,NumSlices] Net Current in cb [ns^-1]
5 NetCurrentCB=I.*NetCurrentCoeff+NcbSCH.*NetCurrentCBCoeff2;
6
7 %[1,NumSlices] Non radiative recombination in SCH [ns^-1]
8 NonRadiativeRecombinationSCH=sqrt(NcbvbSCH).*OneOverTauNRcbSCH;
9
10 %[1,NumSlices] Capture from SCH to WL [ns^-1]
11 CaptureFromSCH2WL=...
12     NcbSCH.*(1-NcbWL.*Number2ProbWLcb).*OneOverTauCapcbSCH2WL;
13 %[1,NumSlices] Escape from WL to SCH [ns^-1]
14 EscapeFromWL2SCH=...
15     NcbWL.*OneOverTauEsccbSCH2WL.*ThermEsc_Barrier_reductionSCH;
16
17 %[1,NumSlices] Tunneling processes from WL to SCH in reversely biased
   slices [ns^-1]
18 TunnelingFromWL2SCH=Tunneling_esc_rateWELL_cb.*NcbWL;
19 %[NumPops,NumSlices] Tunneling processes from ES2 to WL in reversely
   biased slices [ns^-1]
20 TunnelingFromES22SCH=TunnelingEscapeRatecbES2.*NcbES2;
21 %[NumPops,NumSlices] Tunneling processes from ES1 to ES2 in
   reversely biased slices [ns^-1]

```

```

22 TunnelingFromES12SCH=TunnelingEscapeRatecbES1 .* NcbES1 ;
23 %[NumPops,NumSlices] Tunneling processes from GS to ES1 in reversely
    biased slices [ns^-1]
24 TunnelingFromGS2SCH=TunnelingEscapeRatecbGS .* NcbGS ;
25
26 %[1,NumSlices] Variation of carriers in the cb SCH [ns^-1]
27 dNcbSCH= ...
28     NetCurrentCB ...
29     -NonRadiativeRecombinationSCH ...
30     -CaptureFromSCH2WL ...
31     +EscapeFromWL2SCH ...
32     +TunnelingFromWL2SCH ...
33     +sum(TunnelingFromGS2SCH ...
34     +TunnelingFromES12SCH ...
35     +TunnelingFromES22SCH) ;

```

After the SCH, the wetting layer carriers are evaluated. For this state the Auger recombination process has to be considered. As stated when deriving the rate equations, only the neighbouring states are considered for the capture/escape processes, thus for the WL these processes refer to the second excited state (ES2).

$$\begin{aligned}
 \frac{\partial n_{WL}}{\partial t} = & \frac{n_{SCH}}{\tau_{SCH \rightarrow WL}} - \frac{n_{WL}}{\tau_{WL \rightarrow SCH}} - \frac{B_{WL}}{W \cdot h_w} n_{WL}^2 - \frac{n_{WL}}{\tau_{nr,WL}} \\
 & + \sum_{i=1}^N \frac{G_i}{\tau_{WL \rightarrow ES_2}} n_{WL} (1 - \tilde{f}_{ES_2}^i) + \sum_{i=1}^N \frac{n_{ES_2}^i}{\tau_{ES_2 \rightarrow WL}}
 \end{aligned} \tag{A.3}$$

```

1 %%%% Variation of WL carriers %%%%
2 NcbvbWL=NcbWL .* NvbWL ;
3 %[1,NumSlices] rate of non radiative recomb. in WL [ns^-1]
4 NonRadiativeRecombinationWL=sqrt(NcbvbWL) .* OneOverTauNRcbWL ;
5 %[1,NumSlices] rate of spontaneous emission in WL [ns^-1]
6 SpontaneousEmissionWL=Bsp .* NcbvbWL ;
7 %[1,NumSlices] rate of Auger recomb. in WL [ns^-1]
8 AugerRecombinationWL=NcbWL.^3 .* OneOverTauAugerWL ;
9 %[NumPops,NumSlices] rate of capture from ES2 to WL [ns^-1]
10 CaptureFromES22WL=...
11     ((1 - RhocbES2) .* OneOverTauCapcbWL2ES2) .* (InhomDensityES2 .* NcbWL) ;
12 %[NumPops,NumSlices] rate of escape from ES2 to WL [ns^-1]
13 EscapeFromES22WL=...
14     NcbES2 .* OneOverTauEsccbES22WL .* ThermEsc_Barrier_reductionWL ;
15
16 %[1,NumSlices] rate of recombinations in the WL [ns^-1]
17 RecombinationWL=...
18     NonRadiativeRecombinationWL +...
19     SpontaneousEmissionWL +...

```

```

20 AugerRecombinationWL ;
21
22 %[1,NumSlices] Variation of carriers in the cb WL [ns^-1]
23 dNcbWL = ...
24 CaptureFromSCH2WL ...
25 -EscapeFromWL2SCH ...
26 -RecombinationWL ...
27 +sum(EscapeFromES22WL ...
28 -CaptureFromES22WL) ...
29 -TunnelingFromWL2SCH ;

```

ES2 and ES1 carriers variation are subjected to the same processes, but while the first one interacts with the WL and with ES1, the latter interacts with ES2 and the ground state (GS).

$$\begin{aligned}
\frac{\partial n_{ES_2}^i}{\partial t} = & \frac{G_i}{\tau_{WL \rightarrow ES_2}} n_{WL} (1 - \tilde{f}_{ES_2}^i) - \frac{n_{ES_2}^i}{\tau_{ES_2 \rightarrow WL}^i} \\
& - \frac{n_{ES_2}^i}{\tau_{ES_2 \rightarrow ES_1}} (1 - \tilde{f}_{ES_1}^i) + \frac{n_{ES_1}^i}{\tau_{ES_1 \rightarrow ES_2}} (1 - \tilde{f}_{ES_2}^i) \\
& - \frac{n_{ES_2}^i}{\tau_{sp,ES_2}} - \frac{n_{ES_2}^i \tilde{f}_{ES_2}^i}{\tau_{Aug,ES_2}} - \frac{n_{ES_2}^i}{\tau_{nr,ES_2}} - R_{st,ES_2}^i
\end{aligned} \tag{A.4}$$

```

1 %%%% Variation ES2 carriers %%%%
2 %[NumPops,NumSlices] rate of Auger recombination in ES2 [ns^-1]
3 AugerRecombES2 = ...
4 RhovbES2 .* RhocbES2 .* (DotNumberTimesDegOverTauAugercbES2) ;
5
6 %[NumPops,NumSlices] rate of spontaneous emission in ES2 [ns^-1]
7 SpontaneousEmissionES2=NcbES2*OneOverTauSpontES2 ;
8
9 %[NumPops,NumSlices] Non radiative recomb. from ES2 [ns^-1]
10 NonRadiativeRecombES2=NcbES2 .* OneOverTauNRcbES2 ;
11
12 %[NumPops,NumSlices] rate of escape from ES1 to ES2 [ns^-1]
13 EscapeFromES12ES2=NcbES1.*(1 - RhocbES2) .* OneOverTauEscpcbES12ES2 ;
14 %[NumPops,NumSlices] capture rate from ES2 to ES1 [ns^-1]
15 CaptureFromES22ES1=NcbES2.*(1 - RhocbES1) .* OneOverTauCapcbES22ES1 ;
16
17 %[NumPops,NumSlices] Stimulated emission from ES2 [ns^-1]
18 StimulatedEmissionES2 = ...
19 StimulatedEmissionCoeffES2XY .* GainES2 (:, :, cc) .* DeltaEnergyES2 ;
20
21 %[NumPops,NumSlices] rate of recombinations in the ES2 [ns^-1]
22 RecombinationsES2 = ...

```

```

23 NonRadiativeRecombES2+SpontaneousEmissionES2+AugerRecombES2+
    StimulatedEmissionES2;
24
25 %[NumPops, NumSlices] Variation of carriers in the cb ES2 [ns^-1]
26 dNcbES2= ...
27 CaptureFromES22WL ...
28 -RecombinationsES2 ...
29 -EscapeFromES22WL ...
30 +EscapeFromES12ES2 ...
31 -CaptureFromES22ES1 ...
32 -TunnelingFromES22SCH;

```

$$\begin{aligned}
\frac{\partial n_{ES_1}^i}{\partial t} = & \frac{n_{ES_2}^i}{\tau_{ES_2 \rightarrow ES_1}} (1 - \tilde{f}_{ES_1}^i) - \frac{n_{ES_1}^i}{\tau_{ES_1 \rightarrow ES_2}} (1 - \tilde{f}_{ES_2}^i) \\
& - \frac{n_{ES_1}^i}{\tau_{ES_1 \rightarrow GS}} (1 - \tilde{f}_{GS}^i) + \frac{n_{GS}^i}{\tau_{GS \rightarrow ES_1}} (1 - \tilde{f}_{ES_1}^i) \\
& - \frac{n_{ES_1}^i}{\tau_{sp,ES_1}} - \frac{n_{ES_1}^i \tilde{f}_{ES_1}^i}{\tau_{Aug,ES_1}} - \frac{n_{\lambda,ES_1}^i}{\tau_{nr,ES_1}} - R_{st,ES_1}^i
\end{aligned} \tag{A.5}$$

```

1 %%%% Variation ES1 carriers %%%%
2 %[NumPops, NumSlices] rate of Auger recombination in ES1 [ns^-1]
3 AugerRecombES1 = ...
4 RhovbES1 .* RhocbES1 .* DotNumberTimesDegOverTauAugercbES1;
5
6 %[NumPops, NumSlices] rate of spontaneous emission in ES1 [ns^-1]
7 SpontaneousEmissionES1=NcbES1*OneOverTauSpontES1;
8
9 %[NumPops, NumSlices] rate of escape from GS to ES1 [ns^-1]
10 EscapeFromGS2ES1=NcbGS.*(1 - RhocbES1) .* OneOverTauEscbGS2ES1;
11 %[NumPops, NumSlices] capture rate from ES1 to GS [ns^-1]
12 CaptureFromES12GS=NcbES1.*(1 - RhocbGS) .* OneOverTauCapcbES12GS;
13
14 %[NumPops, NumSlices] Non radiative recomb. from ES1 [ns^-1]
15 NonRadiativeRecombES1=NcbES1*OneOverTauNRcbES1;
16
17 %[NumPops, NumSlices] Stimulated emission from ES1 [ns^-1]
18 StimulatedEmissionES1 = ...
19 StimulatedEmissionCoeffES1XY .* GainES1 (:, :, cc) .* DeltaEnergyES1;
20
21 %%[1, NumSlices] rate of recombinations in the ES1 [ns^-1]
22 RecombinationsES1 = ...
23 NonRadiativeRecombES1+AugerRecombES1+SpontaneousEmissionES1+
    StimulatedEmissionES1;
24
25 %[NumPops, NumSlices] Variation of carriers in the cb ES1 [ns^-1]

```

```

26 dNcbES1= ...
27   CaptureFromES22ES1 ...
28   -RecombinationsES1 ...
29   -EscapeFromES12ES2 ...
30   +EscapeFromGS2ES1 ...
31   -CaptureFromES12GS ...
32   -TunnelingFromES12SCH ;

```

Lastly the variation of carriers for the GS (dNcbGS) is evaluated.

$$\begin{aligned}
\frac{\partial n_{GS}^i}{\partial t} = & \frac{n_{ES_1}^i}{\tau_{ES_1 \rightarrow GS}} (1 - \tilde{f}_{GS}^i) - \frac{n_{GS}^i}{\tau_{GS \rightarrow ES_1}} (1 - \tilde{f}_{ES_1}^i) \\
& - \frac{n_{GS}^i}{\tau_{sp,GS}} - \frac{n_{GS}^i \tilde{f}_{h,GS}^i}{\tau_{Aug,GS}} - \frac{n_{GS}^i}{\tau_{nr,GS}} - R_{st,GS}^i
\end{aligned} \tag{A.6}$$

```

1 %%%%% Variation GS carriers %%%%%
2 %[NumPops,NumSlices] rate of Auger recombination in GS [ns^-1]
3 AugerRecombGS = ...
4   RhovbGS .* RhocbGS .* DotNumberTimesDegOverTauAugercbGS ;
5
6 %[NumPops,NumSlices] rate of spontaneous emission in WL [ns^-1]
7 SpontaneousEmissionGS=NcbGS*OneOverTauSpontGS ;
8
9 %[NumPops,NumSlices] Stimulated emission from GS [ns^-1]
10 StimulatedEmissionGS = ...
11   StimulatedEmissionCoeffGSXY .* GainGS(:, :, cc) .* DeltaEnergyGS ;
12
13 %[NumPops,NumSlices] Non radiative recomb. from GS [ns^-1]
14 NonRadiativeRecombGS1=NcbGS*OneOverTauNRcbGS ;
15
16 %[NumPops,NumSlices] rate of recombinations in the GS [ns^-1]
17 RecombinationsGS = ...
18   NonRadiativeRecombGS1+SpontaneousEmissionGS+StimulatedEmissionGS+
19   AugerRecombGS ;
20
21 %[NumPops, NumSlices] variation of GS carriers [-]
22 dNcbGS = ...
23   CaptureFromES12GS ...
24   -RecombinationsGS ...
25   -EscapeFromGS2ES1 ...
26   -TunnelingFromGS2SCH ;

```

After the evaluation of the variation of carriers has been completed, the total number of carriers is computed, and the occupation probabilities are re-evaluated.

```

1  %[1,NumSlices] Number of carriers for SCH in cb [-]
2  NcbSCH=NcbSCH+Sim.subsampleRE*Sim.dt*dNcbSCH;
3  %[1,NumSlices] Number of carriers for WL in cb [-]
4  NcbWL=NcbWL+Sim.subsampleRE*Sim.dt*dNcbWL; NcbWL(NcbWL<0)=0;
5  %[NumPops,NumSlices] Number of carriers for ES2 in cb [-]
6  NcbES2=NcbES2+Sim.subsampleRE*Sim.dt*dNcbES2;
7  %[NumPops,NumSlices] Number of carriers for ES1 in cb [-]
8  NcbES1=NcbES1+Sim.subsampleRE*Sim.dt*dNcbES1;
9  %[NumPops,NumSlices] Number of carriers for GS in cb [-]
10 NcbGS=NcbGS+Sim.subsampleRE*Sim.dt*dNcbGS;
11
12 %[NumPops,NumSlices] Occupation probability for ES2 in vb [-]
13 RhocbES2=NcbES2./DotNumberByDegeneracyES2;
14 %[NumPops,NumSlices] Occupation probability for ES1 in vb [-]
15 RhocbES1=NcbES1./DotNumberByDegeneracyES1;
16 %[NumPops,NumSlices] Occupation probability for GS in vb [-]
17 RhocbGS=NcbGS./DotNumberByDegeneracyGS;

```

Since the implemented model is excitonic, all the values obtained for the conduction band of the device can be simply replicated for the valence band:

```

1  %[1,NumSlices] Number of carriers for SCH in vb[-]
2  NvbSCH=NcbSCH;
3  %[1,NumSlices] Number of carriers for WL in vb [-]
4  NvbWL=NcbWL;
5  %[NumPops,NumSlices] Number of carriers for ES2 in vb [-]
6  NvbES2=NcbES2;
7  %[NumPops,NumSlices] Number of carriers for ES1 in vb [-]
8  NvbES1=NcbES1;
9  %[NumPops,NumSlices] Number of carriers for GS in vb [-]
10 NvbGS=NcbGS;
11
12 %[NumPops,NumSlices] Occupation probability for ES2 in vb [-]
13 RhovbES2=RhocbES2;
14 %[NumPops,NumSlices] Occupation probability for ES1 in vb [-]
15 RhovbES1=RhocbES1;
16 %[NumPops,NumSlices] Occupation probability for GS in vb [-]
17 RhovbGS=RhocbGS;
18 %[1,NumSlices] Net Current in vb [ns^-1]
19 NetCurrentVB=NetCurrentCB;

```

These calculations are repeated in every single time step of the process.

## A.6 Reference energy

The reference energy plays a key role in the developed code, but also in every post-processing script that is used for the graphical representation of the obtained results. In the existing TDTW model that was used as starting point of this work the reference energy was evaluated as follows:

```

1 % [1,1] Transition energy for the ES1 of the central population [eV]
2 PeakEnergyES1=Data . EnergyGapQDCentralPop (end-1);
3 % [1,1] Transition energy for the GS of the central population [eV]
4 PeakEnergyGS=Data . EnergyGapQDCentralPop (end);
5
6 if strcmp (Sim . reference_frequency , 'GS')
7     ReferenceEnergy=PeakEnergyGS;
8 else
9     ReferenceEnergy=(PeakEnergyES1+PeakEnergyGS) / 2;
10 end

```

This simple approach is not sufficient to deal with chirped structures, thus, after the introduction of ES2 as a confined state, the reference energy choice was changed.

```

1 PeakEnergyES2=sum(Data . EnergyGapQDCentralPop (1 ,:)) / Data . NumDiffDots ;
2 PeakEnergyES1=sum(Data . EnergyGapQDCentralPop (2 ,:)) / Data . NumDiffDots ;
3 PeakEnergyGS=sum(Data . EnergyGapQDCentralPop (3 ,:)) / Data . NumDiffDots ;
4
5 if strcmp (Sim . reference_frequency , 'GS')
6     ReferenceEnergy=PeakEnergyGS;
7 elseif strcmp (Sim . reference_frequency , 'ES1')
8     ReferenceEnergy=(PeakEnergyES1+PeakEnergyGS) / 2;
9 else
10    ReferenceEnergy=(PeakEnergyES2+PeakEnergyGS) / 2;
11 end

```

One thing that must be taken into account is the fact that with this approach the different multiplicity of each group is not taken into account. Since in this work the numbers of QD layers in each group did not differ greatly from one another this simplification does not lead to any significant difference; but if the code was used to simulate devices with a predominant group (like a 10-3-3 distribution) the different multiplicity should be taken into account, in the following way:

```

1 PeakEnergyES2=sum(Data . EnergyGapQDCentralPop (1 ,:)) .* Mult) / sum(Mult) ;
2 PeakEnergyES1=sum(Data . EnergyGapQDCentralPop (2 ,:)) .* Mult) / sum(Mult) ;
3 PeakEnergyGS=sum(Data . EnergyGapQDCentralPop (3 ,:)) .* Mult) / sum(Mult) ;

```

The effects of this simplification would be even more prominent if the energy levels were more spaced between them, like a setup in which different materials are used in different groups. To better show this difference and the missing impact on the simulations performed in this work the values obtained with the two approaches, with the parameters of the simulated device, can be observed in table A.1: It can be easily

Reference	Reference Energy [eV]	Reference Energy [eV]
GS	0.9955	0.99834
ES1	1.0242	1.0268
ES2	1.051	1.0528

**Table A.1:** Reference energy without considering multiplicity (center) and considering it (right) for the simulated device

noticed that the difference between the two approaches leads to an error lower than 1%, thus it did not have an impact on the simulations. Grater errors can be observed in Table A.2, where, using the same energy levels, the groups were redistributed in a 10-3-3 setup: With this configuration the errors are of some percentage point, but could still

Reference	Reference Energy [eV]	Reference Energy [eV]
GS	0.9955	1.0141
ES1	1.0242	1.0411
ES2	1.051	1.0628

**Table A.2:** Reference energy without considering multiplicity (center) and considering it (right) with the simulated chirped structure, but with greater asymmetry between the number of layers in each group

be considered negligible. In order to show the possible effects of this misinterpretation, in Table A.3 the reference energies obtained for a system in which the first group has energies 0.5 eV higher than the others is reported. The last considerations are made without making references to any particular material or structure, but serve as an example of errors that could be obtained if the wrong method of picking the reference energy was used.

---

Reference	Reference Energy [eV]	Reference Energy [eV]
GS	1.1622	1.3987
ES1	1.1908	1.4257
ES2	1.2177	1.4474

---

**Table A.3:** Reference energy without considering multiplicity (center) and considering it (right) with great asymmetry between the number of layers in each group and with greater asymmetry in the energy levels

# Bibliography

- [1] G. Fiol, D. Arsenijevic, H. Schmeckeber, C. Meuer, S. Mikhrin, D. Livshits, and D. Bimberg. «Mode-Locked Quantum-Dot Lasers». In: *IEEE Winter Topicals 2011*. IEEE, Jan. 2011. DOI: 10.1109/photwtm.2011.5730035 (cit. on p. 1).
- [2] M.G. Thompson et al. «10 GHz hybrid modelocking of monolithic InGaAs quantum dot lasers». In: *Electronics Letters* 39.15 (2003), p. 1121. DOI: 10.1049/el:20030734 (cit. on p. 1).
- [3] M. Kuntz, G. Fiol, M. Laemmlin, C. Meuer, and D. Bimberg. «High-Speed Mode-Locked Quantum-Dot Lasers and Optical Amplifiers». In: *Proceedings of the IEEE* 95.9 (Sept. 2007), pp. 1767–1778. DOI: 10.1109/jproc.2007.900949 (cit. on p. 1).
- [4] M. Rossetti, P. Bardella, and I. Montrosset. «Time-Domain Travelling-Wave Model for Quantum Dot Passively Mode-Locked Lasers». In: *Quantum Electronics, IEEE Journal of* 47.2 (Feb. 2011), pp. 139–150. ISSN: 0018-9197. DOI: 10.1109/JQE.2010.2055550 (cit. on pp. 1, 4).
- [5] Adam Forrest, M. Krakowski, Paolo Bardella, and Maria Cataluna. «Wide and tunable spectral asymmetry between narrow and wide facet outputs in a tapered quantum-dot superluminescent diode». In: *Optics Express* 28 (Dec. 2019). DOI: 10.1364/OE.377768 (cit. on pp. 2, 19, 20, 23, 24, 26, 27).
- [6] Paolo Bardella Adam F. Forrest Michel Krakowski and Maria Ana Cataluna. «Double-pass amplification of picosecond pulses with a tapered semiconductor amplifier». In: *Optics Express* 27.21 (Oct. 2019), pp. 30752–30762. DOI: 10.1364/OE.27.030752 (cit. on pp. 2, 20, 30, 32).
- [7] S. Cortez, O. Krebs, and P. Voisin. «Polarization of the interband optical dipole in InAs/GaAs self-organized quantum dots». In: *Physical Review B* 63 (2001), pp. 233306–4 (cit. on p. 4).
- [8] K.L. Silverman, R.P. Mirin, S.T. Cundiff, and Norman A.G. «Direct measurement of polarization resolved transition dipole moment in InGaAs/GaAs quantum dots». In: *Applied Physics Letters* 82.25 (June 2003), p. 4552 (cit. on p. 4).

- [9] S. Franchi, G. Trevisi, L. Seravalli, and P. Frigeri. «Quantum dot nanostructures and molecular beam epitaxy». In: *Progress in Crystal Growth and Characterization of Materials* 47.2-3 (2003), pp. 166–195. ISSN: 0960-8974. DOI: DOI : 10 . 1016 / j . pcrysgrow . 2005 . 01 . 002 (cit. on p. 5).
- [10] M. Sugawara. *Self-assembled InGaAs/GaAs quantum dots*. Semiconductors and semimetals. Academic Press, 1999. ISBN: 9780127521695 (cit. on p. 5).
- [11] Zainab Faydh and Ali Fattah. *Digital Signal Processing for Cancellation of Fiber Optic Impairments*. Jan. 2013 (cit. on p. 5).
- [12] M. Krakowski, P. Resneau, M. Calligaro, M. Hugues, M. Hopkinson, M. Gioannini, P. Bardella, and I. Montrosset. «High power, broad spectral width, 1300 nm quantum-dot superluminescent diodes». In: *Semiconductor Laser Conference, 2008. ISLC 2008. IEEE 21st International* (Sept. 2008), pp. 23–24. DOI: 10 . 1109 / ISLC . 2008 . 4635990 (cit. on p. 5).
- [13] V.M. Ustinov et al. «InAs/InGaAs quantum dot structures on GaAs substrates emitting at 1.3  $\mu\text{m}$ ». In: *Applied Physics Letters* 74.19 (May 1999), pp. 2815–2817. ISSN: 0003-6951. DOI: 10 . 1063 / 1 . 124023 (cit. on p. 5).
- [14] B. Tilma, M. Tahvili, J. Kotani, R. Nötzel, M. Smit, and E. Bente. «Measurement and analysis of optical gain spectra in 1.6 to 1.8  $\mu\text{m}$  InAs/InP (100) quantum-dot amplifiers». In: *Optical and Quantum Electronics* 41 (2009), pp. 735–749 (cit. on p. 5).
- [15] N. Marcuvitz. *Waveguide Handbook*. IET, 1951 (cit. on p. 6).
- [16] J. Sieber, U. Bandelow, H. Wenzel, M. Wolfrum, and H. J. Wunsche. *Travelling Wave Equations for Semiconductor Lasers with Gain Dispersion*. Preprints of the Weierstrass Institut für Angewandte Analysis und Stochastik. 1998 (cit. on p. 6).
- [17] P. Blood, H. Pask, H.D. Summers, and I. Sandall. «Localized Auger Recombination in Quantum-Dot Lasers». In: *Quantum Electronics, IEEE Journal of* 43.12 (Dec. 2007), pp. 1140–1146. ISSN: 0018-9197. DOI: 10 . 1109 / JQE . 2007 . 907541 (cit. on p. 9).
- [18] M. Sugawara, H. Ebe, N. Hatori, M. Ishida, Y. Arakawa, T. Akiyama, K. Otsubo, and Y. Nakata. «Theory of optical signal amplification and processing by quantum-dot semiconductor optical amplifiers». In: *Phys. Rev. B* 69.23 (June 2004), p. 235332. DOI: 10 . 1103 / PhysRevB . 69 . 235332 (cit. on p. 11).
- [19] M. Gioannini and I. Montrosset. «Numerical Analysis of the Frequency Chirp in Quantum-Dot Semiconductor Lasers». In: *Quantum Electronics, IEEE Journal of* 43.10 (Oct. 2007), pp. 941–949. ISSN: 0018-9197. DOI: 10 . 1109 / JQE . 2007 . 904306 (cit. on p. 11).

- [20] A. Markus, M. Rossetti, V. Calligari, D. Chek-Al-Kar, J. X. Chen, A. Fiore, and R. Scollo. «Two-state switching and dynamics in quantum dot two-section lasers». In: *Journal of Applied Physics* 100.11 (Dec. 2006), pp. 113104–113104–5. ISSN: 0021-8979. DOI: 10.1063/1.2397293 (cit. on p. 11).
- [21] M Sugawara, T Akiyama, N Hatori, Y Nakata, H Ebe, and H Ishikawa. «Quantum-dot semiconductor optical amplifiers for high-bit-rate signal processing up to 160 Gb·s<sup>-1</sup> and a new scheme of 3R regenerators». In: *Measurement Science and Technology* 13.11 (2002), p. 1683 (cit. on p. 11).
- [22] Charles H. Henry and Rudolf F. Kazarinov. «Quantum noise in photonics». In: *Rev. Mod. Phys.* 68.3 (July 1996), pp. 801–853. DOI: 10.1103/RevModPhys.68.801 (cit. on p. 13).
- [23] Klaus Bohringer and Ortwin Hess. «A full-time-domain approach to spatio-temporal dynamics of semiconductor lasers. I. Theoretical formulation». In: *Progress in Quantum Electronics* 32.5-6 (2008), pp. 159–246. ISSN: 0079-6727. DOI: DOI:10.1016/j.pquantelec.2008.10.002 (cit. on p. 13).
- [24] L.A. Coldren and S.W. Corzine. *Diode lasers and photonic integrated circuits*. Wiley series in microwave and optical engineering. Wiley, 1995. ISBN: 9780471118756 (cit. on p. 13).
- [25] Guotong Du et al. «The monolithic integration of a superluminescent diode with a power amplifier». In: *Photonics Technology Letters, IEEE* 10 (Feb. 1998), pp. 57–59. DOI: 10.1109/68.651102 (cit. on p. 22).